

Role of Internal Motions and Molecular Geometry on the NMR Relaxation of Hydrocarbons

P. M. Singer, D. Asthagiri, Z. Chen, Arjun V. Parambathu, G. J. Hirasaki, and W. G. Chapman

*Department of Chemical and Biomolecular Engineering,
Rice University, 6100 Main St., Houston, TX 77005, USA*

(Dated: September 1, 2021)

The role of internal motions and molecular geometry on ^1H NMR relaxation times $T_{1,2}$ in hydrocarbons is investigated using MD (molecular dynamics) simulations of the autocorrelation functions for intramolecular $G_R(t)$ and intermolecular $G_T(t)$ ^1H - ^1H dipole-dipole interactions arising from rotational (R) and translational (T) diffusion, respectively. We show that molecules with increased molecular symmetry such as neopentane, benzene, and isooctane show better agreement with traditional hard-sphere models than their corresponding straight-chain n -alkane, and furthermore that spherically-symmetric neopentane agrees well with the Stokes-Einstein theory. The influence of internal motions on the dynamics and $T_{1,2}$ relaxation of n -alkanes are investigated by simulating rigid n -alkanes and comparing with flexible (i.e. non-rigid) n -alkanes. Internal motions cause the rotational and translational correlation-times $\tau_{R,T}$ to get significantly shorter and the relaxation times $T_{1,2}$ to get significantly longer, especially for longer-chain n -alkanes. Site-by-site simulations of ^1H 's along the chains indicate significant variations in $\tau_{R,T}$ and $T_{1,2}$ across the chain, especially for longer-chain n -alkanes. The extent of the stretched (i.e. multi-exponential) decay in the autocorrelation functions $G_{R,T}(t)$ are quantified using inverse Laplace transforms, for both rigid and flexible molecules, and on a site-by-site bases. Comparison of $T_{1,2}$ measurements with the site-by-site simulations indicate that cross-relaxation (partially) averages-out the variations in $\tau_{R,T}$ and $T_{1,2}$ across the chain of long-chain n -alkanes. This work also has implications on the role of nano-pore confinement on the NMR relaxation of fluids in the organic-matter pores of kerogen and bitumen.

Keywords: Intramolecular relaxation, Intermolecular relaxation, BPP theory, Rigid molecules, Cross-relaxation

I. INTRODUCTION

Recent studies have shown that MD (molecular dynamics) simulations can successfully predict ^1H NMR (nuclear magnetic resonance) relaxation times $T_{1,2}$ and diffusion coefficients of bulk hydrocarbons and water, without any adjustable parameters in the interpretation of the simulation data [1]. Besides validating the forcefields used in the simulations, the MD simulations reveal new insight about the NMR relaxation from intramolecular versus intermolecular ^1H - ^1H dipole-dipole interactions in fluids, which are not easily accessible experimentally [2]. For instance, the simulations quantify the relative strength of the two relaxation mechanisms, indicating that intramolecular increasingly dominates over intermolecular relaxation with increasing molecular chain-length (i.e. increasing carbon number). This validates the common practice of only considering intramolecular dipole-dipole interactions for simulations of macromolecules such as proteins [3] or polymers in the short-time regime [4].

However, as also reported in [1], the *functional forms* of the simulated autocorrelation functions for intramolecular $G_R(t)$ (i.e. rotational) and intermolecular $G_T(t)$ (i.e. translational) ^1H - ^1H dipole-dipole interactions show significant deviations from the traditional hard-sphere models by Bloembergen, Purcell, Pound (BPP) [5] and Torrey [6], respectively. In the case of intramolecular interactions, the BPP model predicts a single-exponential decay for $G_R(t)$ with rotational-

correlation time τ_R however, the simulations clearly indicate an increasingly “stretched” (i.e. multi-exponential) decay with increasing chain-length. For intermolecular interactions, the Torrey model predicts a specific functional form for $G_T(t)$ (and an associated translational-correlation time τ_T), however, the simulations also indicate a “stretched” decay at large chain-lengths. Another prediction from the hard-sphere models [5, 6] is that the ratio of translational-diffusion correlation-time τ_D (where $\tau_D = \frac{5}{2}\tau_T$) [7] to rotational-correlation time τ_R should be $\tau_D/\tau_R = 9$ [8], which we show in this report is the case for spherically-symmetric neopentane. However, the simulations clearly show that $\tau_D/\tau_R \ll 9$ at large chain-lengths [1]. These findings indicate that the Stokes-Einstein radius for rotational and translational motion are comparable for short-chain and spherical alkanes, but increasingly diverge with increasing chain length, indicating limitations of ascribing a single “radius” for chain molecules.

While the molecular dynamics of long-chain n -alkanes are expected to deviate from hard-sphere predictions, the underlying theory for the deviations remain elusive and difficult to verify experimentally. Simplified models for the autocorrelation function of non-spherical and non-rigid molecules have been successfully developed in the past, such as those by Woessner and others which describe spin-relaxation processes in two-proton systems undergoing anisotropic reorientation [9–11] and internal motions [12], as well as three-proton systems [13]. These anisotropic reorientation models have been successful for highly symmetric molecules such as benzene, where

in-plane and perpendicular-to-plane rotational diffusion-coefficients (and rotational correlation-times) can be determined from NMR measurements and MD simulations [14, 15]. In the case of *intramolecular* (i.e. rotational) relaxation for molecules of lower symmetry, such theories result in a multi-exponential decay for the autocorrelation function $G_R(t)$, with a corresponding distribution in correlation times. Generalizations of such models for the autocorrelation function later arose which take a “model free” or heuristic approach to the internal motions, such as the Lipari-Szabo model [16, 17] often used in polymers [18] and proteins [19]. However, as the internal motions of the molecule become more complex, one is invariably forced to develop even more heuristic models of the autocorrelation function and its associated spectral density [20, 21]. Such heuristic approaches include a variety of distribution functions for the underlying correlation times, including the Cole-Davidson distribution function [4, 22], the generalized gamma function [18], the Kohlrausch-Williams-Watts [4] functions, and the Singer-Hirasaki function [23], each chosen to fit the observations, but without theoretical justification. In the case of bulk water (which exhibits hydrogen-bonding), $G_R(t)$ is stretched to a similar extent as *n*-pentane [1], which may be a result of large, discrete angular-jumps [24] superimposed on a continuous-time rotational-diffusion process [25].

In this report, we study the influence of internal motions and molecular geometry on the molecular dynamics of hydrocarbons by simulating the autocorrelation functions $G_{R,T}(t)$ of rigid *n*-alkanes (i.e. without internal motions), compared with flexible *n*-alkanes (i.e. with internal motions). While such rigid *n*-alkanes do not exist in nature, they present an ideal testing ground for simulating the influence of internal motions on correlation times and relaxation times. We also report site-by-site simulations $G_{R,T}(t)$ for the ^1H 's across the chain, thereby quantifying the underlying distribution in correlation times $\tau_{R,T}$ and relaxation times $T_{1,2}$ across the molecule. The simulations of both the rigid molecules and the site-by-site ^1H 's reveal key insights about the functional forms of $G_{R,T}(t)$ as a function of chain length, without invoking any heuristic models. The site-by-site simulations are also compared with $T_{1,2}$ measurements in the case of *n*-decane and *n*-heptadecane, which show that cross-relaxation [26, 27] partially (in the case of *n*-heptadecane) averages out the underlying variations in $\tau_{R,T}$ and $T_{1,2}$. Such comparisons between measurement and site-by-site simulation could in principle be used as a new method for determining the cross-relaxation rates at low magnetic-fields, provided the proper theoretical framework is developed.

Besides addressing the fundamental science of molecular dynamics of bulk fluids, the present work also opens up new opportunities for investigating the effects of nanometer confinement on fluids, such as the light (i.e. low-viscosity) hydrocarbons confined in the organic-matter pores of the kerogen and bitumen typically found

in organic-rich shale [28, 29]. There is increasing evidence that the NMR surface relaxation of the light hydrocarbons confined in such organic nano-pores is dominated by *intramolecular* [30] and *intermolecular* [31] ^1H - ^1H dipole-dipole interactions, as opposed to surface paramagnetism. Provided the molecular dynamics of the bulk fluid is well understood, the MD simulations of ^1H - ^1H dipole-dipole interactions can then in principle be used to characterize the complex NMR response of fluids confined in organic nano-pores [30–50], which as of yet is not well understood. The effects of nano-confinement on fluids in organic shale can also affect the phase behavior and partitioning of components between the matrix and production fractures as a result of the strong interaction between the fluid molecules and pore surface. It is clear that the fundamental understanding of such complex systems would significantly improve by integrating NMR measurements, MD simulations, and molecular DFT (density functional theory) [51] techniques.

The rest of the article is organized as follows. Section II presents the methodology including: the hydrocarbons investigated and labeled in Section II A, the MD simulation background in Section II B, and the autocorrelation function and NMR relaxation background in Section II C. Section III presents the results and discussions including: the symmetric molecules and hard-sphere models in Section III A, the internal motions in flexible versus rigid molecules in Section III B, the site-by-site simulations and distribution in correlation times in Section III C, including the cross-relaxation effects and comparison with measurements in Section III C 1. Conclusions are presented in Section IV.

II. METHODOLOGY

This section introduces the hydrocarbons under investigation, and presents a brief review of the MD simulations, the definition and properties of the autocorrelation functions, and, the derivation of the NMR relaxation times. Further information about the methodology can be found in [1].

A. Hydrocarbons investigated and labeled

The hydrocarbons simulated in this report are shown in Fig. 1. Neopentane (C_5H_{12}) refers to the isomer 2,2-dimethylpropane, and is labeled “oC5” for short; it is spherically symmetric, and all ^1H 's are topologically equivalent. Benzene (C_6H_6) is labeled as “aC6” for short; it is planar symmetric, and all ^1H 's are equivalent. Cyclohexane (C_6H_{12}) is labeled as “cC6” for short; it contains two inequivalent ^1H 's sites, namely axial and equatorial. Isooctane (C_8H_{18}) refers to the isomer 2,2,4-trimethylpentane, and is labeled “iC8” for short; it is more spherical than the normal isomer *n*-octane (or “nC8 for short), with many inequivalent ^1H 's. The other *n*-

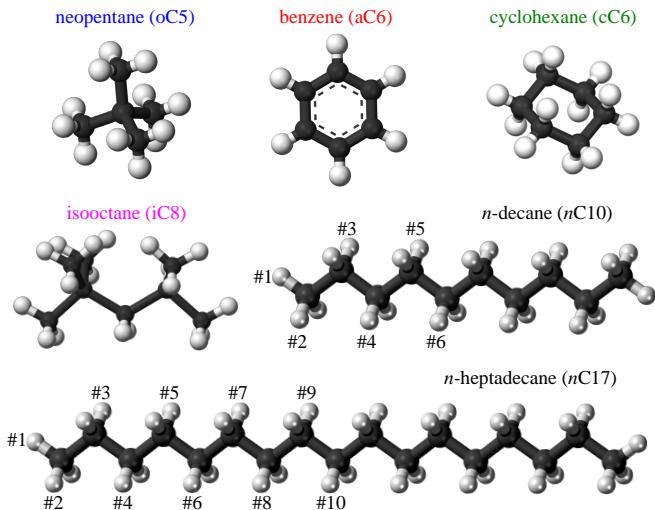


FIG. 1. Ball-and-stick illustrations of the hydrocarbons simulated in this report, including (in order of increasing molar mass): (1) neopentane C_5H_{12} (2,2-dimethylpropane) or “oC5” for short, (2) benzene C_6H_6 or “aC6” for short, (3) cyclohexane C_6H_{12} or “cC6” for short, (4) isooctane C_8H_{18} (2,2,4-trimethylpentane) or “iC8” for short, (5) *n*-decane $n-C_{10}H_{22}$ or “nC10” for short, and (6) *n*-heptadecane $n-C_{17}H_{36}$ or “nC17” for short. *n*-decane and *n*-heptadecane also show labels for the inequivalent 1H ’s along the chain. The other *n*-alkanes (not shown) are labeled *nC*# for carbon number *C*#.

alkanes (not shown) are labeled *nC*# for carbon number *C*#.

The site-by-site simulations are conducted on *n*-decane ($n-C_{10}H_{22}$) labeled as “nC10” for short, and *n*-heptadecane ($n-C_{17}H_{36}$) labeled as “nC17” for short. In the case of *n*-decane, sites #2 \leftrightarrow #6 have a degeneracy of 4, while #1 has a degeneracy of 2. In the case of *n*-heptadecane, sites #2 \leftrightarrow #9 have a degeneracy of 4, while #1 and #10 have a degeneracy of 2. These degeneracies are used to compute the weighted average of the autocorrelation functions. The site-by-site simulations are also conducted on rigid *n*-decane, with the same labels as flexible *n*-decane.

B. Molecular dynamics simulation

The MD simulations of all the flexible hydrocarbons were performed using NAMD [52] version 2.11. The bulk alkanes were modeled using the CHARMM General Force field (CGenFF) [53]. The protocol for setting-up the initial simulation configuration was exactly as before [1]. We use the *n*-alkane simulation trajectory from the earlier work for the analysis noted below. For the cyclic alkanes and isooctane, as before, we created the initial simulation system by packing *N* copies of the molecule into a cube of volume L^3 using the Packmol program

[54]. The volume was chosen such that the number density N/V corresponds to the experimentally determined number density at 293.15 K. The simulation approach for these systems using NAMD was as before [1].

All the rigid body simulations are performed within LAMMPS [55]. For the rigid *n*-alkanes, we took the initial configuration from our earlier work, i.e. the configuration obtained after the Packmol packing procedure. At this stage, by construction all the *n*-alkanes are in the fully extended (all-trans) configuration. Then using the CHARMM-to-LAMMPS tool from the Enhanced Monte Carlo package [56], we prepared the molecular configuration and forcefield information into a LAMMPS input data file. To remove potential steric overlaps from the packing procedure, within LAMMPS we first run 30 steps of constant energy molecular dynamics using the NVE/LIMIT 0.1 option. (The LIMIT option enforces the maximum distance a particle can move and allows the simulation to proceed despite possible overlaps.) Initial velocities for the MD simulation are obtained with a Gaussian distribution and are adjusted to give a temperature of 293.15 K. We find that 30 steps is more than sufficient to remove any potential steric overlaps and also avoid distorting the geometry of the alkanes from their original all-trans configuration. After this dynamics step, we run rigid body molecular dynamics simulations using the RIGID/NVE/SMALL MOLECULE option within LAMMPS. The system is thermostated using a Langevin thermostat with a damping coefficient of 5 ps^{-1} . The cutoff within LAMMPS was exactly as it was in our earlier NAMD runs for the flexible molecules. Specifically, the Lennard-Jones interactions were terminated at 14.00 Å by smoothly switching to zero starting at 13.00 Å. The time step for integrating the equations of motion is 1 fs and the equilibration phase was over 1 ns. In the subsequent production phase, we remove the thermostat. The production phase lasted at least 1 ns and configurations are saved every 100 steps to obtain at least 10^4 frames for analysis. As before [1], the average temperature in the rigid body simulations is within ± 3 K of the target temperature of 293.15 K (20°C).

C. Autocorrelation function and NMR relaxation

The theory of NMR relaxation in liquids is well known [5–8, 57, 58], and the expressions for the autocorrelation functions for *isotropic* intramolecular $G_R(t)$ and *intermolecular* $G_T(t)$ 1H - 1H dipole-dipole interactions are derived in Ref. [1]. Cross-correlation effects are neglected, which is generally justified for isotropic systems [27]. We use the convention based on the text by Mc-

Connell [57], with $G_{R,T}(t)$ in units of s^{-2} :

$$G_{R,T}(t) = \frac{3}{16} \left(\frac{\mu_0}{4\pi} \right)^2 \hbar^2 \gamma^4 \frac{1}{N_{R,T}} \times \sum_{i \neq j}^{N_{R,T}} \left\langle \frac{(3 \cos^2 \theta_{ij}(t + \tau) - 1)}{r_{ij}^3(t + \tau)} \frac{(3 \cos^2 \theta_{ij}(\tau) - 1)}{r_{ij}^3(\tau)} \right\rangle_{\tau}. \quad (1)$$

The correlation times $\tau_{R,T}$ are derived from the following expressions [7]:

$$\tau_{R,T} = \frac{1}{G_{R,T}(0)} \int_0^{\infty} G_{R,T}(t) dt. \quad (2)$$

In other words, $\tau_{R,T}$ is defined as the normalized area under the autocorrelation functions $G_{R,T}(t)$. The areas in this report are determined using Simpson's rule, as opposed to the trapezoidal rule used previously [1]. All flexible n -alkane data in Sections III A and III B are taken from [1], and interpreted using Simpson's rule.

Besides the correlation time, the other parameter of interest is the "second-moment" $\Delta\omega_{R,T}^2$ given by the following expression [7]:

$$G_{R,T}(0) = \frac{1}{3} \Delta\omega_{R,T}^2. \quad (3)$$

The dipolar strength $\Delta\omega_{R,T}$ of the dipole-dipole interaction is derived from Eqs. 1 and 3 to yield the following expression:

$$\Delta\omega_{R,T} = \sqrt{\frac{9}{16} \left(\frac{\mu_0}{4\pi} \right)^2 \hbar^2 \gamma^4 \frac{1}{N_{R,T}} \sum_{i \neq j}^{N_{R,T}} \left\langle \frac{(3 \cos^2 \theta_{ij}(\tau) - 1)^2}{r_{ij}^6(\tau)} \right\rangle_{\tau}}. \quad (4)$$

The simulated $\Delta\omega_{R,T}$ are shown in Fig. 2, in units of kHz. The data indicate that $\Delta\omega_R \simeq 2\Delta\omega_T$ in all cases, except the case of benzene where $\Delta\omega_R \simeq \Delta\omega_T$. The case of benzene can be understood from Eq. 4 since (a) the ^1H coordination number (i.e. the number of nearest neighbors) n_H is smaller and (b) the nearest neighbor ^1H - ^1H distance r_H is larger, therefore $\Delta\omega_R \propto \sqrt{n_H}/r_H^3$ is smaller. In all cases, $\Delta\omega_T$ is roughly the same given that the ^1H spin density is roughly the same. Note that all cases reported here are in the motional averaging regime $\Delta\omega_{R,T} \tau_{R,T} \ll 1$, which is typical of low-viscosity liquids.

The spectral densities $J_{R,T}(\omega)$ (in units of s^{-1}) of the local magnetic-field fluctuations can be determined from the Fourier transform of the autocorrelation function:

$$J_{R,T}(\omega) = 2 \int_0^{\infty} G_{R,T}(t) \cos(\omega t) dt, \quad (5)$$

where $G_{R,T}(t)$ is real and even. In the fast motion regime applicable here (i.e. $\omega_0 \tau_{R,T} \ll 1$, where ω_0 is the Larmor frequency for ^1H), the spectral density follows $J_{R,T}(\omega_0) = J_{R,T}(0)$, and the following can be derived:

$$\frac{1}{T_{1,R,T}} = \frac{1}{T_{2,R,T}} = 5J_{R,T}(0) = \frac{10}{3} \Delta\omega_{R,T}^2 \tau_{R,T}. \quad (6)$$

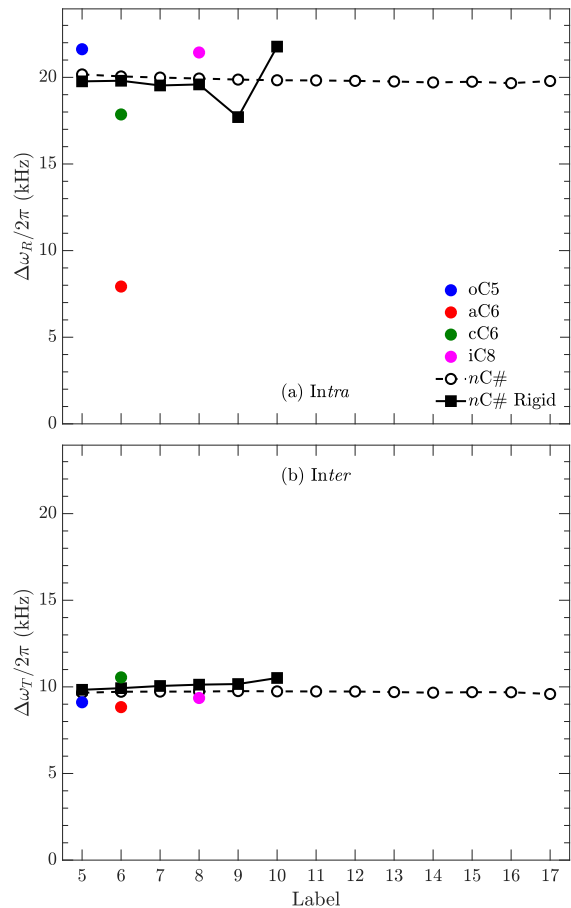


FIG. 2. MD simulation results for the dipolar strength of (a) intramolecular $\Delta\omega_R$ and (b) intermolecular $\Delta\omega_T$ interactions, using Eq. 4 and reported in units of kHz. The hydrocarbon short-hand labels are defined in Fig. 1, and are plotted in order of increasing carbon number $C\#$. $nC\#$ refers to n -alkanes of carbon number $C\#$. "Rigid" refers to rigid hydrocarbons, while all others are flexible. The flexible $nC\#$ data are taken from [1].

In other words, $T_{1,R} = T_{2,R}$ and $T_{1,T} = T_{2,T}$, which is characteristic for low viscosity fluids in the fast motion regime. The total relaxation rates are then equal to the sum of intramolecular and intermolecular rates:

$$\frac{1}{T_1} = \frac{1}{T_2} = \frac{10}{3} \Delta\omega_R^2 \tau_R + \frac{10}{3} \Delta\omega_T^2 \tau_T, \quad (7)$$

which is the final expression used to predict the NMR relaxation time $T_1 = T_2$ from simulation results.

In the case of symmetric molecules such as neopentane, benzene, and methane (CH_4), there is an additional contribution to ^1H NMR relaxation from the spin-rotation interaction [59]. In the case of methane, relaxation from the spin-rotation interaction dominates at low densities (i.e., in the gas phase), whereas relaxation from the ^1H - ^1H dipole-dipole interaction dominates at high densities (i.e. in the liquid phase) [60]. Simulations of the spin-

rotation interaction for these molecules will be reported elsewhere.

In order to quantify the departure of $G_R(t)$ from single-exponential decay, we fit $G_R(t)$ to a sum of multi-exponential decays and determine the underlying distribution in correlation times τ . More specifically, we perform an inversion of the following Laplace transform [61, 62]:

$$\begin{aligned} G_{R,T}(t) &= \int P_{R,T}(\tau) \exp\left(-\frac{t}{\tau}\right) d\tau, \\ G_{R,T}(0) &= \int P_{R,T}(\tau) d\tau, \end{aligned} \quad (8)$$

where $P_{R,T}(\tau)$ (in units of s^{-3}) is the probability distribution function derived from the inversion. Also listed is the integral of $P_{R,T}(\tau)$, which is equal to $G_{R,T}(0)$.

In the case of the BBP hard-sphere model, $P_R(\tau)$ is a delta-function at τ_R , i.e. $P_R(\tau) = G_R(0) \delta(\tau - \tau_R)$. However, as shown by the simulations below, $G_R(t)$ is always stretched (i.e. multi-exponential) to some degree, therefore $P_R(\tau)$ has a finite distribution. The decomposition of $G_{R,T}(t)$ into a sum of exponential decays is common practice in heuristic models of complex molecules [20, 21], where the more complex the molecule dynamics, the more terms are required. This justifies our general approach of decomposing $G_{R,T}(t)$ into a ‘‘model free’’ sum of exponential decays in Eq. 8, for the purposes of quantifying the departure from hard-sphere models.

The $P_{R,T}(\tau)$ distributions were determined by using the discrete form of Eq. 8, using 150 logarithmically-spaced τ bins ranging from 10^{-2} ps $\leq \tau \leq 10^3$ ps, and a fixed regularization parameter $\alpha = 10^{-1}$ [61, 62]. The resulting $P_{R,T}(\tau)$ distributions were then analyzed using the following :

$$\begin{aligned} \mu_{R,T} &= \frac{1}{G_{R,T}(0)} \int P_{R,T}(\tau) \ln(\tau) d\tau, \\ \sigma_{R,T}^2 &= \frac{1}{G_{R,T}(0)} \int P_{R,T}(\tau) (\ln(\tau) - \mu_{R,T})^2 d\tau. \end{aligned} \quad (9)$$

$\sigma_{R,T}$ is the standard deviation and $\mu_{R,T}$ is the mean of the variable $\ln(\tau)$. A natural logarithm in τ is used as the variable since the underlying $P_{R,T}(\tau)$ distributions are discrete and evenly spaced in $\ln(\tau)$.

In the case of n -decane and n -heptadecane, the MD simulation were compared with ^1H T_2 measurements. The n -decane ($\geq 99\%$ purity) and n -heptadecane (99% purity) were obtained from Sigma-Aldrich. The n -alkanes were de-oxygenated by bubbling high-purity N_2 gas overnight and sealing the vial, thereby removing paramagnetic O_2 in solution. The NMR measurements were acquired at ambient conditions ($\simeq 25$ °C) using a GeoSpec2 from Oxford Instruments in an 18 mm probe, at a Larmor frequency of $\omega_0/2\pi = 2.3$ MHz for ^1H (where $\omega_0 = \gamma B_0$, for magnetic-field strength B_0 and gyro-magnetic ratio $\gamma/2\pi = 42.57$ MHz/T for ^1H). A CPMG (Carr-Purcell-Meiboom-Gill) echo train was used with an echo spacing of $T_E = 0.2$ ms, and averaged up

to a signal-to-noise ratio of $\text{SNR} \simeq 10^3$. The $1/T_2$ distributions were determined using a 1D inverse Laplace transform [61, 62], with a regularization parameter of $\alpha \simeq 10^{-3}$ corresponding to the noise floor. The width of the $1/T_2$ distributions was found to be the same at a slightly elevated temperature of 30 °C, which for the case of n -heptadecane rules out any potential influence from the nearby phase-transition at $\simeq 20$ °C.

III. RESULTS AND DISCUSSIONS

A. Symmetric molecules and hard-sphere models

The hard-sphere models developed by BPP [5] and Torrey [6] have been the building blocks for the interpretation of NMR relaxation in liquids. In this section, we show how the case of the more spherical isomers neopentane and isooctane approach the BPP and Torrey theories, and in particular neopentane shows good agreement with the Stokes-Einstein theory. Such agreement validates the hard-sphere theories in a manner never reported before, and at the same time further validates our MD simulation methodology [1].

The *intramolecular* dipole-dipole interaction [5] is traditionally derived using the rotational diffusion equation of rank 2 for hard-spheres of radius R_R , and is parameterized by the rotational diffusion coefficient D_R . The parameter D_R is simply related to rotational correlation time τ_R , which is defined as the average time it takes the molecule to rotate by 1 radian. The *intermolecular* dipole-dipole interaction [6] is traditionally derived using the Brownian motion model where the diffusion propagator is derived for hard-spheres of radius R_T , and is parameterized by the translational diffusion coefficient D_T . The parameter D_T is simply related to the translational-diffusion correlation-time τ_D , which is defined as the average time it takes the molecule to diffuse by one hard-core diameter $2R_T$ [57].

For hard-spheres, the diffusion coefficients (and correlation times) can be related to the bulk properties of the fluid, namely the viscosity η and absolute temperature T , using the traditional Stokes-Einstein relation [8]:

$$\begin{aligned} \tau_R &= \frac{1}{6D_R} = \frac{4\pi}{3k_B} R_R^3 \frac{\eta}{T}, \\ \tau_D &= \frac{2R_T^2}{D_T} = \frac{12\pi}{k_B} R_T^3 \frac{\eta}{T} = \frac{5}{2} \tau_T. \end{aligned} \quad (10)$$

Note that in order to relate the Stokes-Einstein translational-diffusion correlation time τ_D to the NMR derived translational correlation time τ_T (Eq. 2), a factor of $\frac{5}{2}$ is required, i.e. $\tau_D = \frac{5}{2} \tau_T$ [7]. An expression for the two autocorrelation functions are then derived:

$$\begin{aligned} G_R(t) &= G_R(0) \exp\left(-\frac{t}{\tau_R}\right), \\ G_T(t) &= G_T(0) \int_0^\infty 3 \frac{J_{3/2}^2(x)}{x} \exp\left(-x^2 \frac{t}{\frac{5}{2} \tau_T}\right) dx, \end{aligned} \quad (11)$$

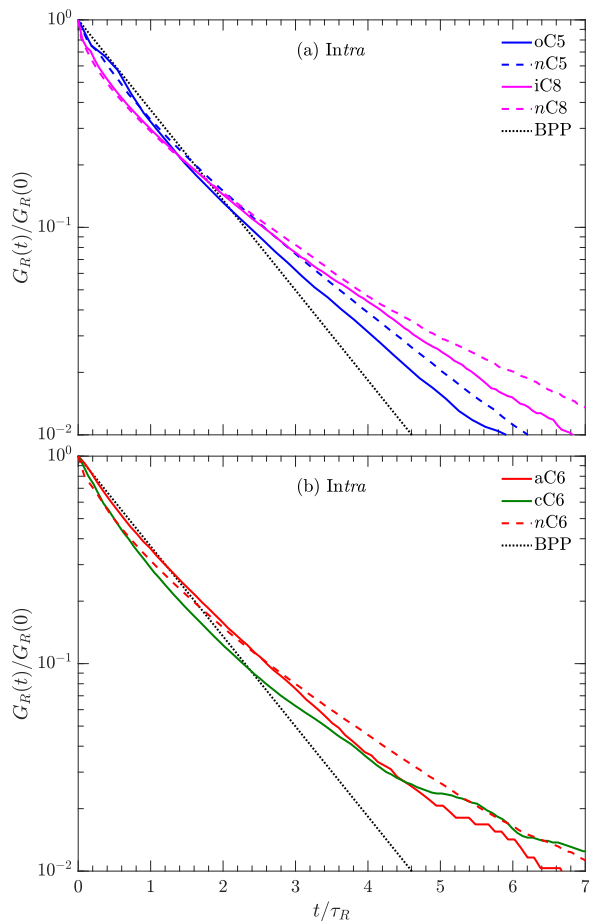


FIG. 3. MD simulations of the autocorrelation function $G_R(t)$ for intramolecular interactions using Eq. 1, for selected hydrocarbons defined in Fig. 1, split into (a) and (b) for clarity. The y -axis has been normalized by zero time value $G_R(0)$, and the x -axis has been normalized by correlation time τ_R (Eq. 2). The prediction from the BPP [5] hard-sphere model (Eq. 11) is shown by the black dotted line.

where both expressions reduce to $G_{R,T}(0)$ (Eq. 3) at $t = 0$.

The BPP hard-sphere model for the intramolecular autocorrelation $G_R(t)$ is plotted in Fig. 3(a) as the dotted black lines. The hard-sphere model is a single-exponential decay (Eq. 11), which is a straight-line decay on the semilog- y plot. The intramolecular $G_R(t)$ appear to be more “stretched” (i.e. multi-exponential) in nature than the hard-sphere model, however neopentane (solid line) is clearly closer to a hard-sphere, relative to the linear isomer n -pentane (dashed line). Similarly, the isooctane (solid line) is closer to the hard-sphere prediction, relative to the linear isomer n -octane (dashed line). These observations are quantified in Fig. 5, where the standard deviation $\sigma_{R,T}$ are plotted for the same dataset as Fig. 2. A more stretched (i.e. multi-exponential) decay in $G_R(t)$ yields a larger distribution $P_R(\tau)$ in cor-

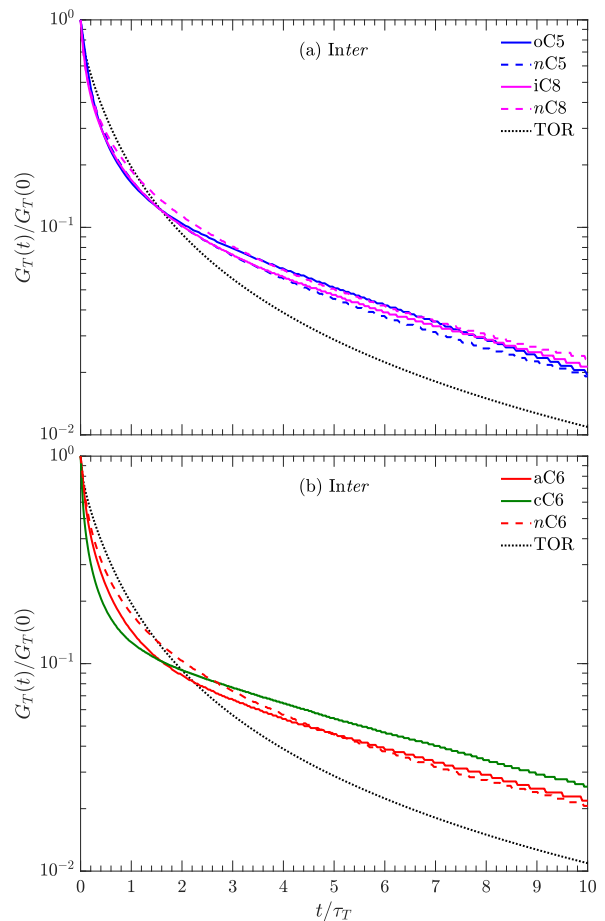


FIG. 4. MD simulations of the autocorrelation function $G_T(t)$ for intermolecular interactions using Eq. 1, for selected hydrocarbons defined in Fig. 1, split into (a) and (b) for clarity. The y -axis has been normalized by zero time value $G_T(0)$, and the x -axis has been normalized by correlation time τ_T (Eq. 2). The prediction from the Torrey [6] (“TOR”) hard-sphere model (Eq. 11) is shown by the black dotted line.

relation times τ (Eq. 8), which yields a larger $\sigma_{R,T}$ (Eq. 9). The BPP hard-sphere model $G_R(t)$ in Eq. 11, on the other hand, predicts a single exponential decay, i.e. $P_R(\tau) = G_R(0) \delta(\tau - \tau_R)$, corresponding to $\sigma_R = 0$ (which is limited to $\sigma_R \simeq 0.038$ in our case due to regularization effects of the inverse Laplace transform [61, 62]). The $P_{R,T}(\tau)$ distributions from the inverse Laplace transform (Eq. 8) used to compute $\sigma_{R,T}$ are shown in Appendix A, including the hard-sphere model. The data in Fig. 5(a) indicate that σ_R drops by $\simeq 27\%$ for neopentane compared to n -pentane; likewise, σ_R drops by $\simeq 22\%$ for isooctane compared to n -octane. This quantifies the observation in Fig. 3 that the more spherical the molecule, the closer to single-exponential decay in $G_R(t)$.

Meanwhile, the Torrey hard-sphere model “TOR” for the intermolecular autocorrelation $G_T(t)$ is plotted in Fig. 4(a) as the dotted black lines. The effect of molec-

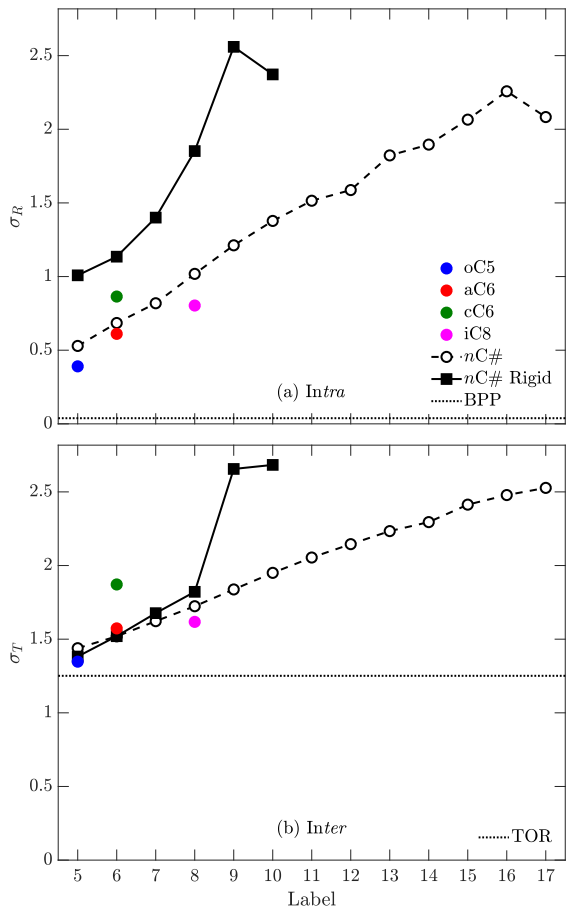


FIG. 5. MD simulation results for the standard deviation of (a) intramolecular σ_R and (b) intermolecular σ_T interactions, using Eq. 9 determined from the $P_{R,T}(\tau)$ distributions (Eq. 8) shown in Appendix A. Same hydrocarbon labels as Fig. 2. Also shown are the BPP model which predicts $\sigma_R = 0$ (or $\simeq 0.038$ in our computation), and the Torrey (TOR) model which predicts $\sigma_T \simeq 1.25$.

ular symmetry does not have a significant effect on the functional form of $G_T(t)$, and remains equally departed from the hard-sphere model. More specifically, the same analysis of $G_T(t)$ in Fig. 4(b) indicates roughly similar σ_T values with molecular symmetry. Note however that the Torrey hard-sphere model (TOR) has a multi-exponential distribution characterized by $\sigma_T \simeq 1.25$. This is due to the fact that $G_T(t)$ in Eq. 11 is not a single exponential decay, even though it contains only one correlation time τ_T (see Appendix A for more details). What is remarkable is that the Torrey hard-sphere prediction $\sigma_T \simeq 1.25$ is consistent with neopentane, and even to some extent n -pentane.

Another way to quantify deviations from the hard-sphere model is to compute the ratio τ_D/τ_R , which according to Eq. 11 should be $\tau_D/\tau_R = 9$ for hard-spheres [8] where the Stokes-Einstein radius for rotation R_R

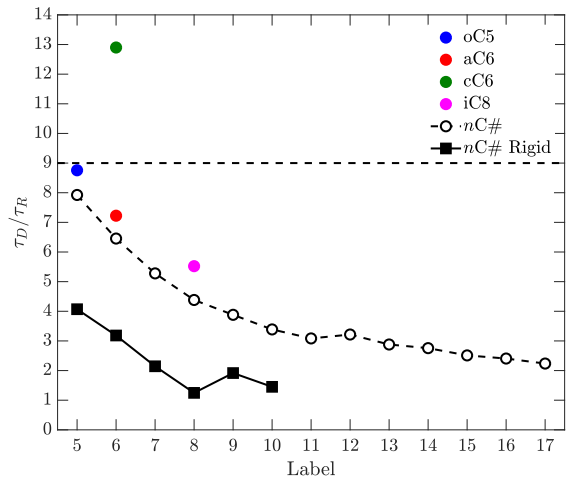


FIG. 6. MD simulation result for ratio τ_D/τ_R of translational-diffusion correlation-time ($\tau_D = \frac{5}{2}\tau_T$) to rotational-correlation time (τ_R), along with predicted value $\tau_D/\tau_R = 9$ [8] from Stokes-Einstein relation (Eq. 10). Same hydrocarbon labels as Fig. 2.

equals the Stokes-Einstein radius for translation R_T . The ratio plotted in Fig. 6 clearly shows that lower n -alkanes tend towards the hard-spheres, while the higher n -alkanes increasingly depart from hard-spheres. Similarly, the ratio for isooctane is found to be closer to a hard-sphere than n -octane, as expected. Furthermore, in the case of neopentane, the ratio is found to be $\tau_D/\tau_R = 8.76$, which is very close to the hard-sphere prediction of 9. This is a remarkable finding which validates the hard-sphere models by BPP, Torrey, and Stokes-Einstein in a manner never reported before.

A similar trend is found for the planar-symmetric molecule benzene, where Fig. 3(b) indicates that benzene (solid line) is closer to the BPP prediction (i.e. straighter) than n -hexane (dashed line). More specifically, as shown in Fig. 5(a), σ_R is found to be $\simeq 10\%$ lower for benzene compared to n -hexane. Likewise, τ_D/τ_R for benzene in Fig. 6 is closer to the hard-sphere prediction of 9 than n -hexane. This indicates that planar-symmetric molecules are more “spherical” than linear chains of the same carbon number, at least when molecular dynamics are concerned.

On the other hand, Fig. 3(b) indicates that cyclohexane (which contains ^1H 's in both axial and equatorial positions) is further away from the BPP prediction (i.e. more stretched) than n -hexane. More specifically, as shown in Fig. 5(a), σ_R is found to be $\simeq 15\%$ higher for cyclohexane compared to n -hexane. Likewise τ_D/τ_R for cyclohexane in Fig. 6 is further away from the hard-sphere prediction of 9 than n -hexane. This indicates that the out of plane ^1H sites in cyclohexane result in larger deviations from hard-spheres than linear chains of the same carbon number.

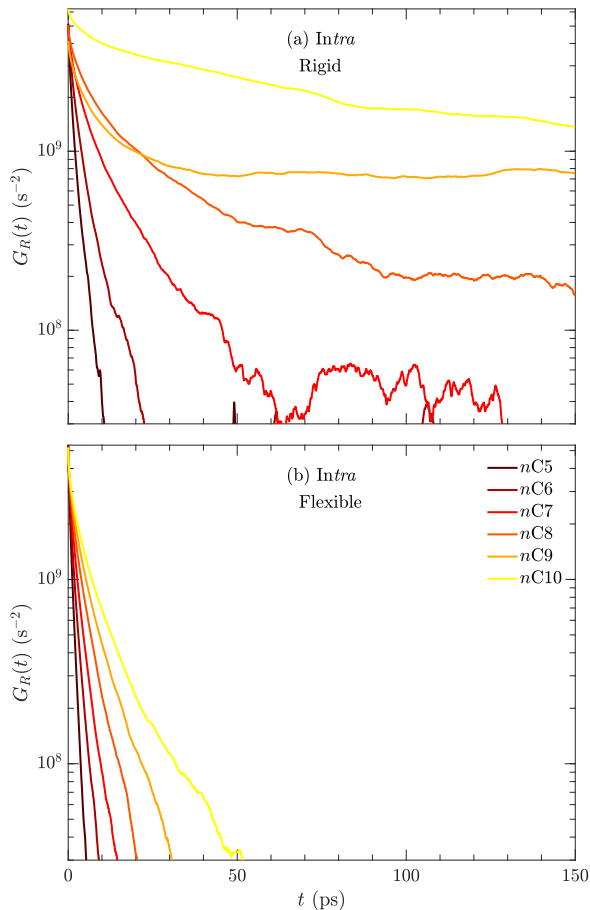


FIG. 7. MD simulations of the autocorrelation function $G_R(t)$ for intramolecular interactions, for (a) rigid and (b) flexible hydrocarbons, from n -pentane ($nC5$) to n -decane ($nC10$).

B. Internal motions in flexible versus rigid molecules

As discussed above, neopentane is a spherical molecule with relatively stiff (i.e. rigid) bonds, and is therefore expected to agree with the above mentioned BPP, Torrey, and Stokes-Einstein theory of hard spheres. We now turn our attention to the effects of internal motions in the long-chain n -alkanes, which we study here by simulating completely rigid n -alkanes. While rigid molecules do not exist in nature, they provide an ideal testing ground for quantifying the effects of rigidity on the molecular dynamics and the NMR relaxation. For convenience, all data in this section and the previous section are listed in the supplementary material.

The characterization of internal motions in hydrocarbons originates from Woessner's theories [12], who postulated that internal motions would decrease the correlation times $\tau_{R,T}$ and therefore increase the relaxation times $T_{1,2}$ in liquids. As here for n -decane, we find that internal motions increase τ_R by a factor $\simeq 12$, resulting

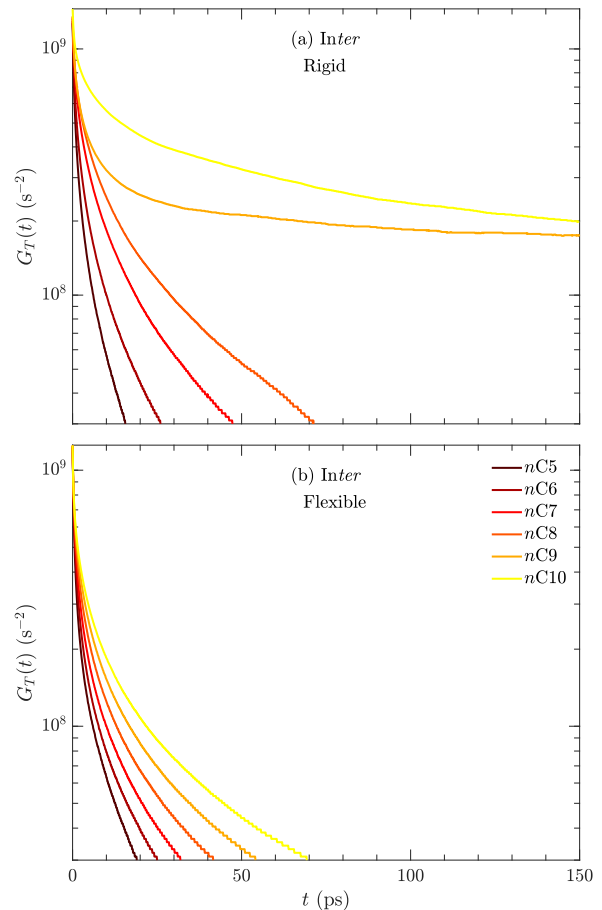


FIG. 8. MD simulations of the autocorrelation function $G_T(t)$ for intermolecular interactions, for (a) rigid and (b) flexible hydrocarbons, from n -pentane ($nC5$) to n -decane ($nC10$).

in a factor $\simeq 13$ decrease in $T_{1,2}$. Furthermore, it was postulated in [12] that internal motions would cause the intramolecular contribution to relaxation to decrease relative to the intermolecular contribution. As shown here for n -alkanes, we find that internal motions decrease the intramolecular contribution relative to the intermolecular contribution by a factor $\simeq 2$, on average. In other words, we can test the original theories using MD simulations, without invoking any heuristic models.

The effects of internal motions on intramolecular autocorrelation functions $G_R(t)$ for $nC5 \leftrightarrow nC10$ are shown in Fig. 7, presented in such a way as to allow for direct comparison between (a) rigid molecules and (b) flexible molecules. The internal motions clearly decrease the correlation times τ_R , as shown when going from (a) rigid to (b) flexible molecules. Likewise, the intermolecular autocorrelation functions $G_T(t)$ for $nC5 \leftrightarrow nC10$ are shown in Fig. 8, and show a similar decrease in correlation times τ_T in going from (a) rigid to (b) flexible. What is also significant is that the stretched decay for intramolecular $G_R(t)$ in Fig. 7 persists for rigid molecules, indicat-

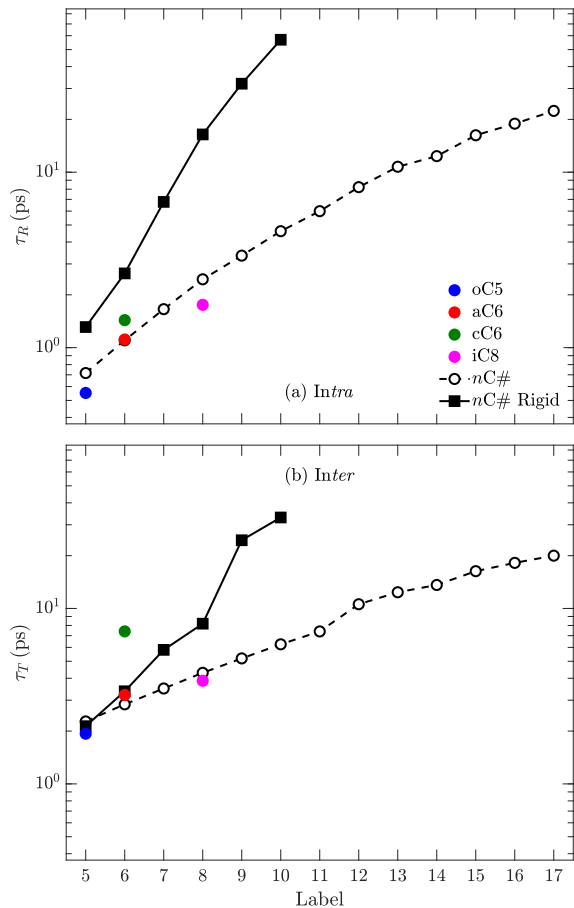


FIG. 9. MD simulation results for correlation times from (a) intramolecular τ_R and (b) intermolecular τ_T interactions, using Eq. 2. Same hydrocarbon labels as Fig. 2.

ing that molecular geometry plays a crucial role in the functional-form for $G_R(t)$. If internal motions were the only cause of the stretched decay, then the functional forms for rigid $G_R(t)$ (which do not have internal motions) would be straighter (i.e. closer to single exponential). In fact the opposite is found, namely the standard deviation σ_R is a factor $\simeq 2$ larger for rigid molecules compared to flexible molecules, as shown in Fig. 5(a). This suggests that internal motions have a tendency to narrow the underlying distribution $P_R(\tau)$ (Eq. 8) in correlation times τ .

Meanwhile, the functional forms for intermolecular $G_T(t)$ of rigid molecules in Fig. 8 continues to deviate from the Torrey model, again indicating that molecular geometry also plays a crucial role in the functional-form for $G_T(t)$. As shown in Fig. 5(b), the standard deviation σ_T is a factor $\simeq 2$ larger for rigid $nC9$ and $nC10$ compared to flexible $nC9$ and $nC10$. This suggests that internal motions have a tendency to narrow the underlying distribution $P_T(\tau)$ (Eq. 8) in correlation times, for $nC9$ and above.

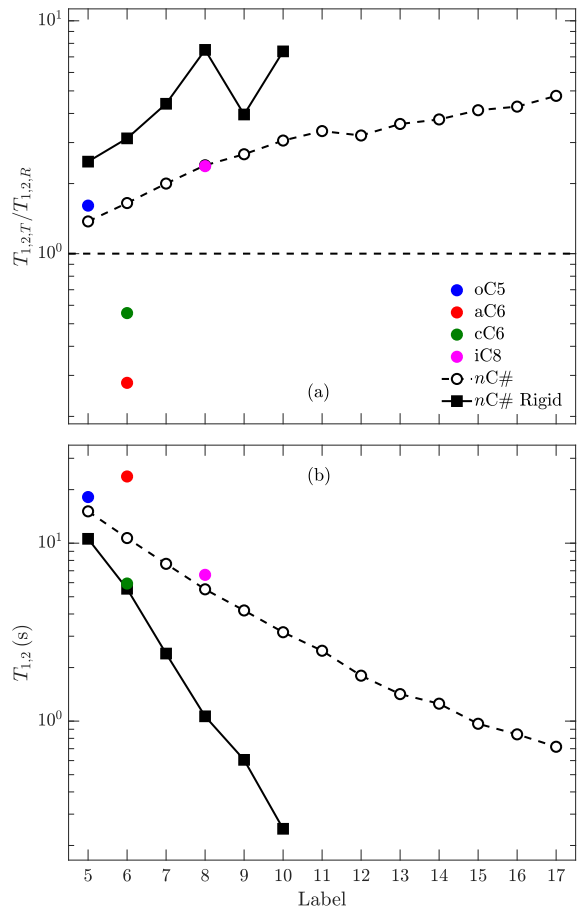


FIG. 10. MD simulation results for (a) the ratio of relaxation times $T_{1,2,T}/T_{1,2,R}$ using Eq. 6, where $T_{1,2,T}/T_{1,2,R} \gg 1$ indicates that intramolecular dominates over intermolecular, and (b) the total relaxation time $T_{1,2}$, using Eq. 7. Same hydrocarbon labels as Fig. 2.

In order to quantify these findings, the same analysis for the dipolar strengths $\Delta\omega_{R,T}$ (Eq. 4) and correlation times $\tau_{R,T}$ (Eq. 2) is applied to the rigid molecules. In the case of $\Delta\omega_{R,T}$, Fig. 2 indicates that rigidity does not significantly effect the dipolar strength. In the case of $\Delta\omega_R$ this is expected since on average over time, the nearest neighbor ^1H 's are the same distance apart for both rigid and flexible, i.e. the equilibrium positions are the same. It is evident however that the rigid $\Delta\omega_R$ simulation shows some scattering of the order $\pm 10\%$ at large chain-lengths. Likewise, $\Delta\omega_T$ remains roughly the same since the density of rigid and flexible fluids are the same, implying that the ^1H spin density is roughly the same.

The correlation times $\tau_{R,T}$ computed using Eq. 2 for rigid and flexible molecules are plotted in Fig. 9 for (a) intramolecular and (b) intermolecular interactions. The rotational correlation-time τ_R for flexible benzene agrees well with previous estimates from NMR measurements and MD simulations [14, 15]. In the case of rigid

molecules, the maximum autocorrelation time $t = 150$ ps did not fully capture the decay in $G_{R,T}(t)$, implying that $\tau_{R,T}$ is underestimated for rigid n C9 and rigid n C10, and $T_{1,2}$ is correspondingly overestimated for rigid n C9 and rigid n C10. Nevertheless, Fig. 9(a) shows that the estimated intramolecular τ_R is a factor $\simeq 2$ greater for rigid n C5 than flexible n C5, and a factor $\simeq 12$ greater for rigid n C10 than flexible n C10. Meanwhile, Fig. 9(b) shows that the estimated intermolecular τ_T is roughly the same between rigid n C5 and flexible n C5, but a factor $\simeq 5$ greater for rigid n C10 than flexible n C10. These findings clearly imply that internal motion effects become more prominent with increasing chain-length.

The next step is to compute the corresponding relaxation times from the $\Delta\omega_{R,T}$ and $\tau_{R,T}$ data using Eq. 6. Fig. 10(a) shows the ratio in relaxation times $T_{1,2,T}/T_{1,2,R}$, where $T_{1,2,T}/T_{1,2,R} \gg 1$ indicates that intramolecular relaxation dominates over intermolecular relaxation, while $T_{1,2,T}/T_{1,2,R} \ll 1$ indicates that intermolecular dominates over intramolecular instead. The data indicates that internal motions decrease the intramolecular contribution relative to the intermolecular contribution by a factor $\simeq 2$ on average, although some scattering exists in the $T_{1,2,T}/T_{1,2,R}$ data for rigid n C9 and rigid n C10. This is consistent with the predictions in [12]. These results can also be viewed as the ratio τ_D/τ_R (where $\tau_D = \frac{5}{2}\tau_T$) in Fig. 6, which shows that τ_D/τ_R for rigid molecules is on average by a factor $\simeq 2$ further away from the hard-sphere model. This indicates that rigid n -alkanes are less “spherical” than flexible n -alkanes, as might be expected.

Finally, Fig. 10(b) presents the total relaxation time $T_{1,2}$ computed using Eq. 7, showing that $T_{1,2}$ is a factor $\simeq 1.4$ shorter for rigid n C5 than flexible n C5, while it is a factor $\simeq 13$ shorter for rigid n C10 than flexible n C10. Again, these findings clearly imply that internal motions effects become more prominent with increasing chain-length, in line with predictions from [12].

It should be noted in passing that for the flexible isomers discussed in Section III A, Fig. 10 shows that while neopentane and isooctane show results consistent with their corresponding n -alkane, benzene and cyclohexane clearly do not. Specifically, Fig. 10(a) shows that for all cases $T_{1,2}$ relaxation is dominated by intramolecular interactions, i.e. $T_{1,2,T}/T_{1,2,R} \gg 1$, *except* for benzene and cyclohexane which show that $T_{1,2}$ is dominated by intermolecular interactions instead, i.e. $T_{1,2,T}/T_{1,2,R} \ll 1$. In the case of benzene, this is a result of a lower $\Delta\omega_R$ (Fig. 2(a)) compared to all the other n -alkanes. In the case of cyclohexane, this is a result of a larger τ_T (Fig. 9(b)) compared to n -hexane. These difference result in the spread of $T_{1,2}$ (Fig. 10(b)) for benzene and cyclohexane compared with n -hexane.

C. Site-by-site simulations and distribution in correlation times

The above results show that internal motions are not the primary cause of the stretched decay. Our next task is therefore to determine whether the multi-exponential decay in $G_R(t)$ (and the deviations in $G_T(t)$ from the Torrey model) are a result of underlying variations in molecular dynamics across the chain-length. This scenario was postulated previously, where the fast rotation (i.e. short τ_R) of the methyl groups act as relaxation sinks for the macro-molecule [27]. For convenience, all data in this section are listed in the supplementary material.

In order to investigate variations across the chain, we perform the MD simulations for each ^1H across the chain, and then compute the correlation times $\tau_{R,T}$ and relaxation times $T_{1,2}$ on a site-by-site basis across the chain. The ^1H sites are labeled in Fig. 1 for n -decane and n -heptadecane, where the #1 ^1H is on the methyl end-group, and the largest number is in the middle of the chain (more details in Section II A). Intramolecular $G_R(t)$ for n -heptadecane in Fig. 11(a) shows a large distribution in correlation times, with the #1 and #2 ^1H 's on the methyl clearly having the steepest decay (i.e. shortest τ_R), as expected from [27]. The average “Ave” is the weighted average over all sites, and constitutes what was reported in the previous sections. Meanwhile, intermolecular $G_T(t)$ for n -heptadecane in Fig. 11(b) shows less variation between sites than intramolecular, which is intuitive since the distance of closest approach between molecules should be roughly independent of the location along the chain. The same site-by-site method is used for n -decane. Both the intramolecular $G_R(t)$ for n -decane in Fig. 12(a) and the intermolecular $G_T(t)$ for n -decane in Fig. 12(b) show less variation between sites than n -heptadecane. This is intuitive since one expects there to be more variation in the molecular dynamics across longer chains.

A more quantitative summary of the site-by-site correlation times $\tau_{R,T}$ (using Eq. 2) is given in Fig. 13, for both n -decane and n -heptadecane. In the case of n -heptadecane, the ^1H 's labeled #1 and #2 (both on the methyl end-group) show a factor $\simeq 4$ shorter intramolecular τ_R than at the middle of the chain, and a factor $\simeq 1.4$ shorter intermolecular τ_T . In the case of n -decane, #1 and #2 show a factor $\simeq 2$ shorter intramolecular τ_R than at the middle of the chain, and a factor $\simeq 1.4$ shorter intermolecular τ_T . Also shown in Fig. 13 are results from the site-by-site simulation for rigid n -decane. It is interesting to note that for rigid n -decane, #1 and #2 only show a factor $\simeq 1.4$ shorter intramolecular τ_R than the chain middle, which is somewhat less variation than for flexible n -decane. In other words, the internal motions have a tendency to enhance the site-by-site variation of intramolecular τ_R across the chain. In the case of intermolecular τ_T , both rigid and flexible n -decane (as well as flexible n -heptadecane) show

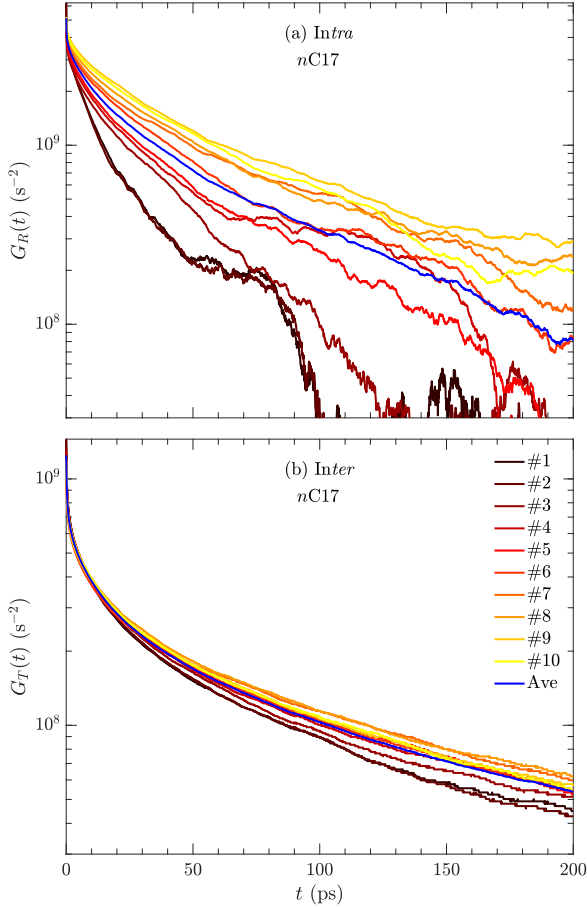


FIG. 11. MD simulation results of the autocorrelation function for (a) intramolecular $G_R(t)$ and (b) intermolecular $G_T(t)$ interactions using Eq. 1, for n -heptadecane ($nC17$) on a site-by-site basis with labels defined in Fig. 1. “Ave” indicates weighted average over the site-by-site results.

the same factor $\simeq 1.4$ shorter τ_T for #1 and #2 versus the chain middle, which is reasonable given that the distance of closest approach between molecules should be the same across the chain, regardless of whether the molecule is rigid or not.

Given the large variation in τ_R across the chain (Fig. 13), one expects the average $G_R(t)$ to be a multi-exponential (i.e. stretched) decay, since the average $G_R(t)$ is the weighted sum of decays over all sites. Indeed n -decane (Fig. 12) and n -heptadecane (Fig. 11) show a stretched decay for the average. What is remarkable, however, is that $G_R(t)$ for both n -decane (Fig. 12) and n -heptadecane (Fig. 11) show a stretched decay *at every site*. The extent of the stretched (i.e. multi-exponential) decay can be quantified on a site-by-site basis using $\sigma_{R,T}$ (Eq. 9), in a similar fashion as Section III A. As shown in 14(a), σ_R does not vary significantly across the chain, although the data may indicate a slightly lower value at the chain ends (#1 and #2), for both $nC10$ and $nC17$. The

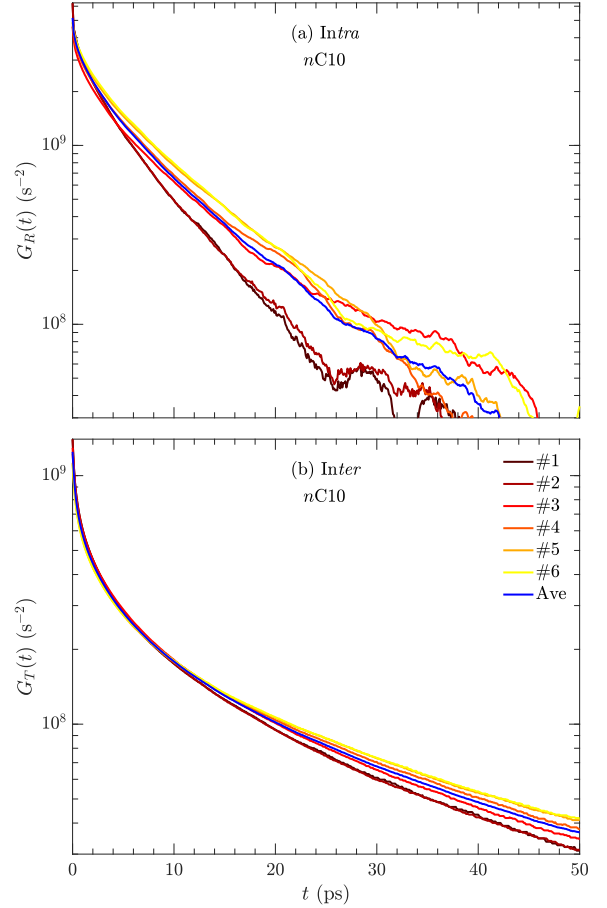


FIG. 12. MD simulation results of the autocorrelation function for (a) intramolecular $G_R(t)$ and (b) intermolecular $G_T(t)$ interactions using Eq. 1, for n -decane ($nC10$) on a site-by-site basis with labels defined in Fig. 1. “Ave” indicates weighted average over the site-by-site results.

fact that σ_R is roughly uniform across the chain implies that not only does each site show a stretched decay, but all the sites show roughly the *same* stretched functional form as the average. Similar results are found for the case of site-by-site $G_R(t)$ for *rigid* n -decane, where Fig. 14(a) shows a roughly uniform σ_R across the rigid chain. All these findings imply that the overall molecular geometry is a crucial factor, perhaps even the *dominant* factor, behind the functional form in the decay of $G_R(t)$.

Similar conclusions can also be made for intermolecular $G_T(t)$ in Figs. 12(b) and 11(b), which clearly show that the site-by-site decays overlap with the average. The same can be inferred from the σ_T data in Fig. 14(b), with even more certainty since σ_T shows less scattering than σ_R .

It is also interesting to track the strength of intramolecular versus intermolecular relaxation on a site-by-site basis across the chain. Fig. 15(a) presents the ratio $T_{1,2,T}/T_{1,2,R}$ across the chain sites, which shows

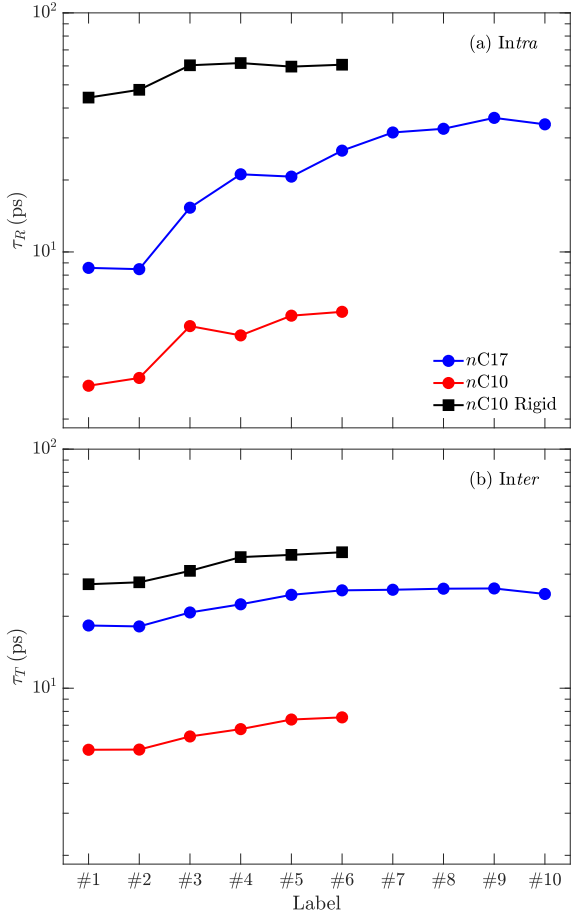


FIG. 13. MD simulation results for correlation times from (a) intramolecular τ_R and (b) intermolecular τ_T interactions, using Eq. 2, on a site-by-site basis with site labels defined in Fig. 1. “Rigid” refers to rigid hydrocarbons, while all others are flexible.

that the intramolecular relaxation dominates in the chain middle (i.e. $T_{1,2,T}/T_{1,2,R} \gg 1$), while intramolecular relaxation is a factor of $\simeq 2$ stronger than intermolecular at the chain ends (i.e. #1 and #2). In the case of *n*-heptadecane, the chain middle shows a factor $\simeq 3$ larger value of $T_{1,2,T}/T_{1,2,R}$ than the chain ends. In the case of *n*-decane, the chain middle shows only a factor $\simeq 1.5$ larger value of $T_{1,2,T}/T_{1,2,R}$ than the chain ends, which is reasonable given the smaller variation in correlation times $\tau_{R,T}$ for *n*-decane (Fig. 13). Rigid *n*-decane shows almost no variation in $T_{1,2,T}/T_{1,2,R} \simeq 7$, and clearly intramolecular relaxation dominates across the entire chain.

Finally, Fig. 15(b) presents the total relaxation time $T_{1,2}$ on a site-by-site basis. In the case of *n*-heptadecane, the chain middle shows a factor $\simeq 3$ shorter value of $T_{1,2}$ than the chain ends. In the case of rigid and flexible *n*-decane, the chain middle shows only a factor $\simeq 1.5$ shorter value of $T_{1,2}$ than the chain ends, which is rea-

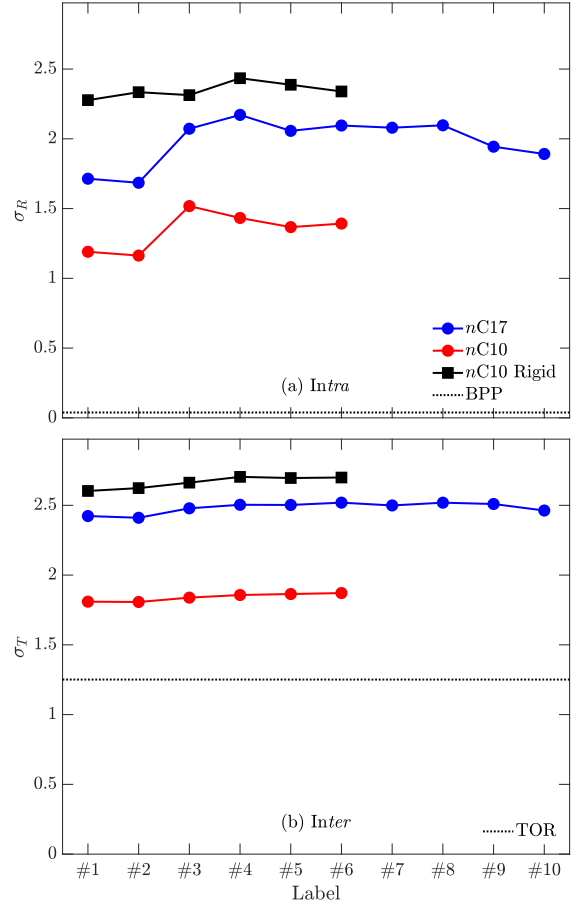


FIG. 14. MD simulation results for the standard deviation of (a) intramolecular σ_R and (b) intermolecular σ_T interactions, using Eq. 9 determined from the $P_{R,T}(\tau)$ distributions (Eq. 8). Same hydrocarbon labels as Fig. 13. Also shown are the BPP model which predicts $\sigma_R = 0$ (or $\simeq 0.038$ in our computation), and the Torrey (TOR) model which predicts $\sigma_T \simeq 1.25$.

sonable given the smaller variation in correlation times $\tau_{R,T}$ in Fig. 13.

1. Cross-relaxation effects and comparison with measurements

Despite the site-by-site variation in correlation times $\tau_{R,T}$ (Fig. 13) and subsequent variation in relaxation times $T_{1,2}$ (Fig. 15(b)) across the chain, the measured distribution in $T_{1,2}$ values for liquids is never as large. This is a result of strong cross-relaxation effects, a.k.a. “spin diffusion” effects, which tend to average out (i.e. “wash out”) any such variations across the chain [27, 63–65].

The condition for either strong, intermediate, or weak cross-relaxation is determined by the relative strength of the cross-relaxation rate $\sigma_{1,2,ij}$ between spin-pairs i

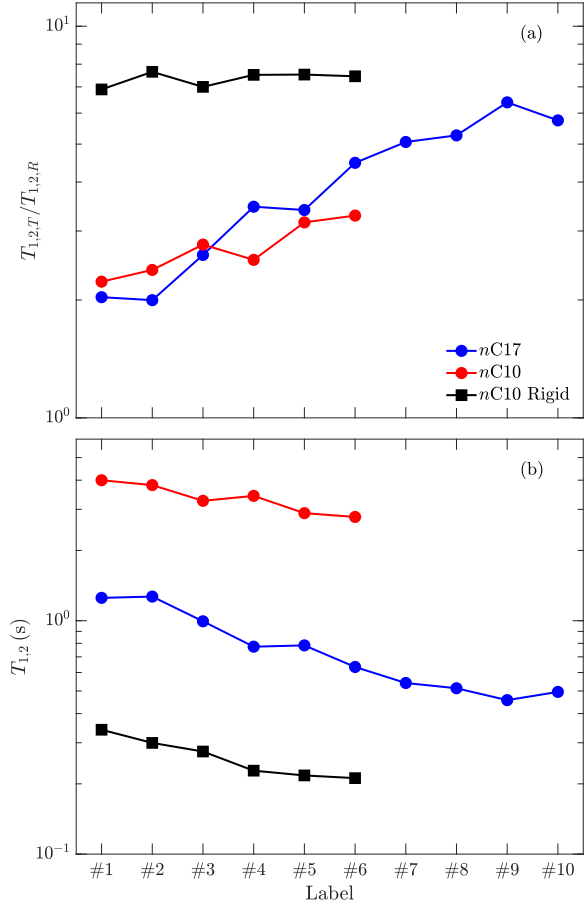


FIG. 15. MD simulation results for (a) the ratio of relaxation times $T_{1,2,T}/T_{1,2,R}$ using Eq. 6, where $T_{1,2,T}/T_{1,2,R} \gg 1$ indicates that intramolecular dominates over intermolecular, and (b) the total relaxation time $T_{1,2}$, using Eq. 7. Same hydrocarbon labels as Fig. 13.

and j compared with the difference in individual relaxation rates $|1/T_{1,2,i} - 1/T_{1,2,j}|$ (see supplementary material for more details). More specifically, the different cross-relaxation regimes can be defined as such [3, 27]:

$$\begin{aligned} \sigma_{1,2,ij} &\gg \frac{1}{2} |1/T_{1,2,i} - 1/T_{1,2,j}| \quad (\text{strong}), \\ \sigma_{1,2,ij} &\simeq \frac{1}{2} |1/T_{1,2,i} - 1/T_{1,2,j}| \quad (\text{intermediate}), \\ \sigma_{1,2,ij} &\ll \frac{1}{2} |1/T_{1,2,i} - 1/T_{1,2,j}| \quad (\text{weak}). \end{aligned} \quad (12)$$

For strong cross-relaxation, which is generally the case for low-viscosity liquids, one expects the measured $T_{1,2}$ to be single-valued and given by the average rate [10, 27]:

$$\frac{1}{T_{1,2}} = \frac{1}{N} \sum_i \frac{1}{T_{1,2,i}}, \quad (13)$$

where N is the number of ^1H 's in the chain, and $1/T_{1,2,i}$ is the relaxation rate of the i 'th ^1H in the chain shown in

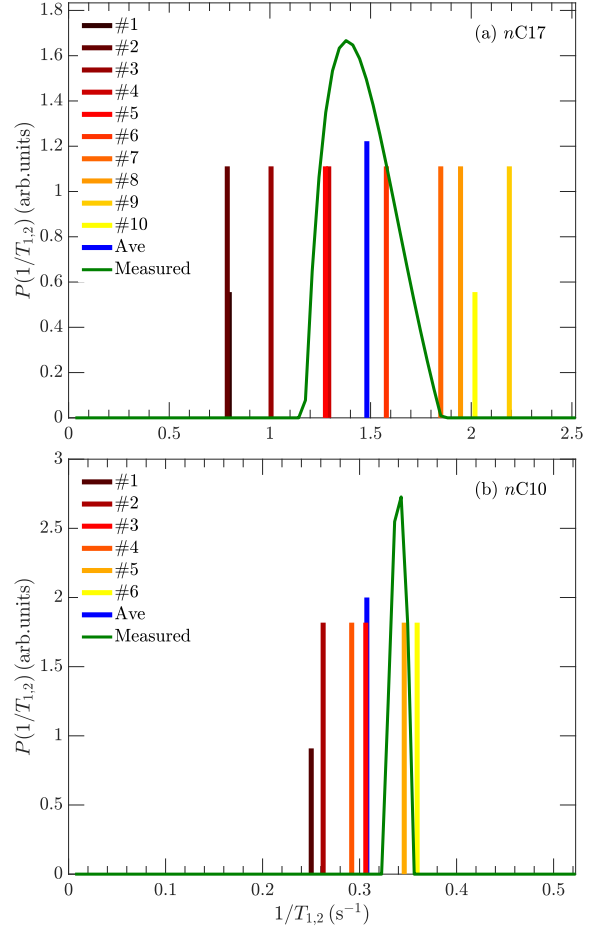


FIG. 16. (a) MD simulation result for distribution in site-by-site values of $1/T_{1,2,i}$ taken from Fig. 15(b), for (a) $n\text{C}17$ and (b) $n\text{C}10$, with labels defined in Fig. 1 and with relative heights according to degeneracy. “Ave” indicates weighted average over the site-by-site results Eq. 13, with arbitrary height. Simulations results are compared with measured distributions of $1/T_2$, with arbitrary height.

Fig. 15(b). One consequence of averaging the relaxation rates in Eq. 13 is that the average $1/T_{1,2}$ is equivalent to computing the weighted average $G_{R,T}(t)$ in Figs. 11 and 12, and then using Eqs. 2–7.

The comparison between simulation and measurements are shown in Fig. 16. In the case of n -heptadecane, the simulation predicts an average value of $1/T_{1,2} \simeq 1.48 \text{ s}^{-1}$, which is close to the measured value of $1/T_{1,2} \simeq 1.45 \text{ s}^{-1}$. In the case of n -decane, the simulation predicts an average value of $1/T_{1,2} \simeq 0.308 \text{ s}^{-1}$, which is also close to the measured value of $1/T_{1,2} \simeq 0.328 \text{ s}^{-1}$. Such agreement was previously reported in [1], which validates our MD simulation methodology.

However, while the mean values agree, Fig. 16 clearly shows that the widths of simulation versus measurement do not agree. In the case of n -heptadecane (Fig. 16(a)), the simulation predicts a width of $\Delta_{1,2} \simeq 1.40 \text{ s}^{-1}$ (de-

defined as the difference between maximum and minimum values in the distribution), which is a factor $\simeq 3$ times larger than the measured full-width at half-maximum $W_{1,2} \simeq 0.42 \text{ s}^{-1}$ of the distribution. The n -heptadecane results therefore indicate that cross-relaxation partially averages out the site-by-site distribution in relaxation. In other words, in the case of weak cross-relaxation $\sigma_{1,2,ij} \ll \frac{1}{2}|1/T_{1,2,i} - 1/T_{1,2,j}|$, the measured $W_{1,2}$ would agree with $\Delta_{1,2} \simeq 1.40 \text{ s}^{-1}$ from simulation. In the case of strong cross-relaxation $\sigma_{1,2,ij} \gg \frac{1}{2}|1/T_{1,2,i} - 1/T_{1,2,j}|$, the measured $W_{1,2}$ would tend towards zero (i.e. the $1/T_{1,2}$ distribution would tend towards a delta function), which in practice will be limited by the experimental resolution of $\simeq 0.06/T_{1,2}$ (as determined on a water sample). Fig. 16(a) indicates that $\sigma_{1,2,ij}$ is somewhere in-between the strong and weak cross-relaxation regime, i.e. in the intermediate regime, suggesting that $\sigma_{1,2,ij}$ could in principle be calculated from the observed difference between simulation and measurements at low magnetic-fields ($\omega_0/2\pi \lesssim 2.3 \text{ MHz}$).

In the case of n -decane (Fig. 16(b)), the simulation predicts a width of $\Delta_{1,2} \simeq 0.11 \text{ s}^{-1}$, which is much larger than the measured $W_{1,2} \simeq 0.02 \text{ s}^{-1}$. Given that the experimental resolution limit has been reached, the true measured width for n -decane must satisfy $W_{1,2} < 0.02 \text{ s}^{-1}$. This implies that $\Delta_{1,2}$ is at least a factor $\gtrsim 6$ times larger than $W_{1,2}$, indicating that cross-relaxation is more efficient for n -decane than for n -heptadecane.

IV. CONCLUSIONS

The traditional hard-sphere models developed by Bloembergen, Purcell, Pound [5] and Torrey [6] continue to be the building blocks in describing NMR relaxation from rotational (R) and translational (T) diffusion of molecules, respectively. The BPP hard-sphere model predicts a single-exponential decay in the autocorrelation function $G_R(t)$, however $G_R(t)$ for the n -alkanes becomes increasingly “stretched” (i.e. multi-exponential) with increasing chain-length [1]. Likewise, $G_T(t)$ shows greater departure from the Torrey hard-sphere model with increasing chain-length [1]. We quantify the departure of $G_R(t)$ from the single-exponential model by fitting $G_R(t)$ to a sum of exponential decays using an inverse Laplace transform, and determine the standard deviation σ_R (i.e. the normalized standard deviation) of the underlying distribution $P_R(\tau)$ in correlation times τ . We find that hydrocarbons of greater molecular symmetry such as neopentane and isooctane have $\simeq 25\%$ lower σ_R than their corresponding linear n -alkanes. Furthermore, in the case of the spherically-symmetric neopentane, we find that the ratio of translational-diffusion to rotational correlation times is found to be $\tau_D/\tau_R = 8.76$ (where $\tau_D = \frac{5}{2}\tau_T$), which agrees well with the Stokes-Einstein prediction of $\tau_D/\tau_R = 9$.

By comparing the relaxation of rigid and flexible n -alkanes, we find a factor $\simeq 12$ increase in the rotational

correlation-time τ_R for rigid n -decane compared with flexible n -decane, together with a factor $\simeq 5$ increase in the translational correlation-time τ_T , thereby revealing the strong influence of internal motions on $\tau_{R,T}$ and $T_{1,2}$ for long-chain n -alkanes. The extent of the stretched (i.e. multi-exponential) decay of $G_{R,T}(t)$ is greater for rigid n -alkanes, namely the $\sigma_{R,T}$ values are a factor $\simeq 2$ larger for rigid compared to flexible n -alkanes, indicating that internal motions tend to narrow the underlying distribution $P_{R,T}(\tau)$ (Eq. 8) in correlation times τ .

We find that $T_{1,2}$ relaxation from intramolecular interactions dominates over intermolecular interactions (i.e. $T_{1,2,T}/T_{1,2,R} \gg 1$) for all hydrocarbons investigated, *except* for benzene and cyclohexane where intermolecular interactions dominate (i.e. $T_{1,2,T}/T_{1,2,R} \ll 1$). The rigid n -alkanes show a factor $\simeq 2$ larger ratio $T_{1,2,T}/T_{1,2,R}$ than flexible n -alkanes, indicating that internal motions somewhat diminish the influence of intramolecular interactions.

Site-by-site simulations of $G_{R,T}(t)$ for the ^1H 's across the chain indicate that τ_R decreases by a factor $\simeq 4$ towards the chain-ends of n -heptadecane, together with a factor $\simeq 1.4$ decrease in τ_T , thereby revealing variations in $\tau_{R,T}$ and $T_{1,2}$ across the chain for long-chain n -alkanes. Moreover, the simulations indicate that the stretched functional-forms of site-by-site $G_{R,T}(t)$ are approximately the *same* as the chain averages, namely the $\sigma_{R,T}$ values are roughly the same across the chain, indicating that the overall molecular geometry plays a crucial (if not dominant) role in the functional-form of the decay in $G_{R,T}(t)$.

Corresponding $T_{1,2}$ measurements of n -heptadecane indicate a narrower distribution in $T_{1,2}$ than site-by-site simulations, implying that cross-relaxation (partially) averages-out the variations in $\tau_{R,T}$ and $T_{1,2}$ across the chain of long-chain n -alkanes. Such $T_{1,2}$ comparisons between site-by-site simulations and measurements at low magnetic-field ($\omega_0/2\pi \lesssim 2.3 \text{ MHz}$) could in principle be used to compute the cross-relaxation rates $\sigma_{1,2,ij}$ for long-chain n -alkanes.

This work informs our on-going work in understanding the NMR relaxation and diffusion of hydrocarbons (and other fluids) in nano-confined pores, such as the light hydrocarbons found in the organic-matter pores of kerogen and bitumen [23, 30, 49] typically found in organic-shale reservoirs.

V. ACKNOWLEDGMENTS

This work was funded by the Rice University Consortium on Processes in Porous Media, and the American Chemical Society Petroleum Research Fund [ACS-PRF-58859-ND6]. We gratefully acknowledge the National Energy Research Scientific Computing Center, which is supported by the Office of Science of the U.S. Department of Energy [DE-AC02-05CH11231], for HPC time and support. We also gratefully acknowledge the Texas

-
- [1] P. M. Singer, D. Asthagiri, W. G. Chapman, and G. J. Hirasaki, *J. Magn. Reson.* **277**, 15 (2017).
- [2] D. E. Woessner, *J. Chem. Phys.* **41** (1), 84 (1964).
- [3] J. Kowalewski and L. Maler, *Nuclear Spin Relaxation in Liquids: Theory, Experiments, and Applications* (Taylor & Francis Group, 2006).
- [4] P. Henritzi, A. Bormuth, and M. Vogel, *Solid State Nucl. Magn. Reson.* **54**, 32 (2013).
- [5] N. Bloembergen, E. M. Purcell, and R. V. Pound, *Phys. Rev.* **73** (7), 679 (1948).
- [6] H. C. Torrey, *Phys. Rev.* **92** (4), 962 (1953).
- [7] B. Cowan, *Nuclear Magnetic Resonance and Relaxation* (Cambridge University Press, 1997).
- [8] A. Abragam, "Principles of nuclear magnetism," (Oxford University Press, International Series of Monographs on Physics, 1961).
- [9] D. E. Woessner, *J. Chem. Phys.* **36** (1), 1 (1962).
- [10] D. E. Woessner, *J. Chem. Phys.* **37** (3), 647 (1962).
- [11] W. T. Huntress, *J. Chem. Phys.* **48** (8), 3524 (1968).
- [12] D. E. Woessner, *J. Chem. Phys.* **42** (6), 1855 (1965).
- [13] P. S. Hubbard, *J. Chem. Phys.* **51** (4), 1647 (1969).
- [14] A. Laaksonen, P. Stilbs, and R. E. Wasylshen, *J. Chem. Phys.* **108** (2), 455 (1998).
- [15] R. Witt, L. Sturz, A. Dolle, and F. Muller-Plathe, *J. Phys. Chem. A* **104**, 5716 (2000).
- [16] G. Lipari and A. Szabo, *J. Amer. Chem. Soc.* **104**, 4546 (1982).
- [17] G. Lipari and A. Szabo, *J. Amer. Chem. Soc.* **104**, 4559 (1982).
- [18] S. Kariyo, A. Brodin, C. Gainaru, A. Herrmann, H. Schick, V. N. Novikov, and E. A. Rossler, *Macromolecules* **41**, 5313 (2008).
- [19] D. Frueh, *Prog. Nucl. Magn. Reson. Spect.* **41**, 305 (2002).
- [20] P. A. Beckmann, *Phys. Rep.* **171** (3), 85 (1988).
- [21] V. I. Bakhmutov, *NMR Spectroscopy in Liquids and Solids* (CRC Press, Taylor & Francis Group, 2015).
- [22] A. Bormuth, M. Hofmann, P. Henritzi, M. Vogel, and E. A. Rossler, *Macromolecules* **46**, 7805 (2013).
- [23] P. M. Singer, Z. Chen, L. B. Alemany, G. J. Hirasaki, K. Zhu, Z. H. Xie, and T. D. Vo, *Energy Fuels*, DOI: 10.1021/acs.energyfuels.7b03603 (2018).
- [24] C. Calero, J. Martı, and E. Guardia, *J. Phys. Chem. B* **119**, 1966 (2015).
- [25] W. A. M. Madhavi, S. Weerasinghe, and K. I. Momot, *J. Phys. Chem. B* **121**, 10893 (2017).
- [26] I. D. Campbell and R. Freeman, *J. Magn. Reson.* **11**, 143 (1973).
- [27] A. Kalk and H. J. C. Berendsen, *J. Magn. Reson.* **24**, 343 (1976).
- [28] Q. R. Passey, K. Bohacs, W. L. Esch, R. Klimentidis, and S. Sinha, *Soc. Petrol. Eng. SPE-131350-MS* (2010).
- [29] R. G. Loucks, R. M. Reed, S. C. Ruppel, and U. Hammes, *AAPG Bull.* **96**, No. 6, 1071 (2012).
- [30] P. M. Singer, Z. Chen, and G. J. Hirasaki, *Petrophysics* **57** (6), 604 (2016).
- [31] K. E. Washburn and Y. Cheng, *J. Magn. Reson.* **278**, 18 (2017).
- [32] A. E. Ozen and R. Sigal, *Petrophysics* **54** (1), 11 (2013).
- [33] E. Rylander, P. M. Singer, T. Jiang, R. E. Lewis, R. McLin, and S. M. Sinclair, *Soc. Petrol. Eng. SPE-164554-MS* (2013).
- [34] T. Jiang, E. Rylander, P. M. Singer, R. E. Lewis, and S. M. Sinclair, *Soc. Petrophys. Well Log Analysts*, SPWLA (2013).
- [35] P. M. Singer, E. Rylander, T. Jiang, R. McLin, R. E. Lewis, and S. M. Sinclair, *Soc. Core Analysts SCA2013-18* (2013).
- [36] K. E. Washburn and J. E. Birdwell, *J. Magn. Reson.* **233**, 17 (2013).
- [37] R. Kausik, K. Fellah, E. Rylander, P. M. Singer, R. E. Lewis, and S. M. Sinclair, *Soc. Core Analysts SCA2014-73* (2014).
- [38] H. Daigle, A. Johnson, J. P. Gips, and M. Sharma, *Unconv. Resources Tech. Conf. URTEC-1905272-MS* (2014).
- [39] K. E. Washburn, *Concepts Magn. Reson. A* **43** (3), 57 (2014).
- [40] J.-P. Korb, B. Nicot, A. Louis-Joseph, S. Bubici, and G. Ferrante, *J. Phys. Chem. C* **118** (40), 23212 (2014).
- [41] B. Nicot, N. Vorapalawut, B. Rousseau, L. F. Madariaga, G. Hamon, and J.-P. Korb, *Petrophysics* **57** (1), 19 (2015).
- [42] M. Lessenger, R. Merkel, R. Medina, S. Ramakrishna, S. Chen, R. Balliet, H. Xie, P. Bhattad, A. Carnerup, and M. Knackstedt, *Soc. Petrophys. Well Log Analysts*, SPWLA (2015).
- [43] J. E. Birdwell and K. E. Washburn, *Energy Fuels* **29**, 2234 (2015).
- [44] M. Fleury and M. Romero-Sarmiento, *J. Petrol. Sci. Eng.* **137**, 55 (2016).
- [45] R. Kausik, K. Fellah, E. Rylander, P. M. Singer, R. E. Lewis, and S. M. Sinclair, *Petrophysics* **57** (4), 339 (2016).
- [46] B. Sun, E. Yang, H. Wang, S. J. Seltzer, V. Montoya, J. Crowe, and T. Malizia, *Soc. Petrophys. Well Log Analysts*, SPWLA (2016).
- [47] C. Sondergeld, A. Tinni, C. Rai, and A. Besov, *Soc. Petrophys. Well Log Analysts*, SPWLA (2016).
- [48] D. Yang and R. Kausik, *Energy Fuels* **30** (6), 4509 (2016).
- [49] Z. Chen, P. M. Singer, J. Kuang, M. Vargas, and G. J. Hirasaki, *Petrophysics* **58** (5), 470 (2017).
- [50] A. Valori, S. V. den Berg, F. Ali, and W. Abdallah, *Energy Fuels* **31**, 5913 (2017).
- [51] J. Liu, L. Wang, S. Xi, D. Asthagiri, and W. G. Chapman, *Langmuir* **33** (42), 11189 (2017).
- [52] J. C. Phillips, R. Braun, W. Wang, E. Tajkhorshid, E. Villa, C. Chipot, R. Skeel, L. Kale, and K. Schulten, *J. Comput. Chem.* **26**, 1781 (2005).
- [53] K. Vanommeslaeghe, E. Hatcher, C. Acharya, S. Kundu, S. Zhong, J. Shim, E. Darian, O. Guvench, P. Lopes, I. Vorobyov, and A. D. M. Jr., *J. Comput. Chem.* **31**,

- 671 (2010).
- [54] L. Martinez, R. Andrade, E. G. Birgin, and J. M. Martinez, *J. Comput. Chem.* **30**, 2157 (2009).
- [55] S. Plimpton, *J. Comput. Phys.* **117**, 1 (1995).
- [56] P. J. in't Veld and G. C. Rutledge, *Macromolecules* **36**, 7358 (2003).
- [57] J. McConnell, "The theory of nuclear magnetic relaxation in liquids," (Cambridge University Press, 1987).
- [58] R. Kimmich, *NMR Tomography, Diffusometry and Relaxometry* (Springer-Verlag, 1997).
- [59] P. S. Hubbard, *Phys. Rev.* **131** (3), 1155 (1963).
- [60] S.-W. Lo, G. J. Hirasaki, W. V. House, and R. Kobayashi, *Soc. Petrol. Eng. J.* **7** (1), 24 (2002).
- [61] L. Venkataramanan, Y.-Q. Song, and M. D. Hürlimann, *IEEE Transactions on Signal Processing* **50** (5), 1017 (2002).
- [62] Y.-Q. Song, L. Venkataramanan, M. D. Hürlimann, M. Flaum, P. Frulla, and C. Straley, *J. Magn. Reson.* **154**, 261 (2002).
- [63] I. Solomon, *Phys. Rev.* **99** (2), 559 (1955).
- [64] H. T. Edzes and E. T. Samulski, *Nature* **265**, 521 (1977).
- [65] J. B. Lambert and E. P. Mazzola, *Nuclear Magnetic Resonance Spectroscopy: An Introduction to Principles, Applications, and Experimental Methods* (Prentice-Hall, 2004).

APPENDIX A

As mentioned in Section III A, the probability distribution functions $P_{R,T}(\tau)$ of correlation time τ are shown in Figs. 17 and 18. The $P_{R,T}(\tau)$ are derived from the inverse Laplace transforms in Eq. 8 of the $G_{R,T}(t)$ simulations in Figs. 3 and 4, respectively. The $P_{R,T}(\tau)$ are then used to derive the coefficients of variance $\sigma_{R,T}$ using Eq. 9. For instance, it is clear from Figs. 17 and 18 that $P_{R,T}(\tau)$ are narrower for neopentane, benzene and isooctane (i.e. have lower $\sigma_{R,T}$) compared to their corresponding straight-chain n -alkane, respectively.

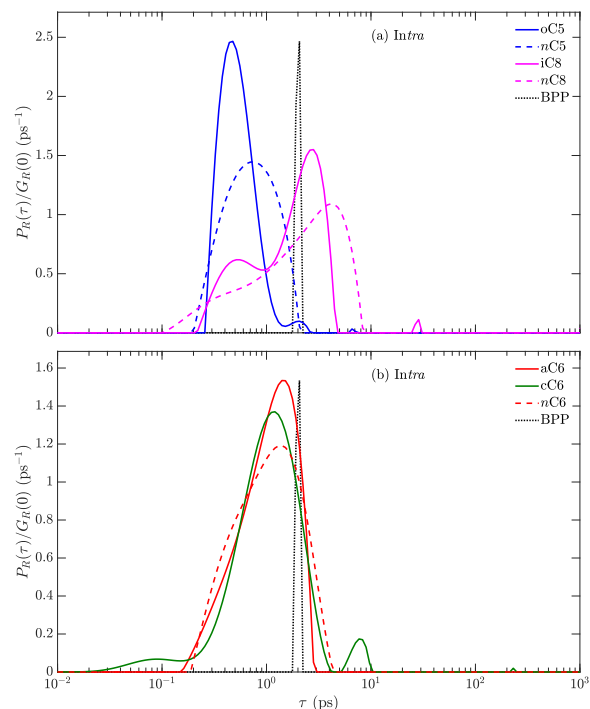


FIG. 17. Probability distribution function $P_R(\tau)$ of rotational correlation time τ derived from the inverse Laplace transform (Eq. 8) of the $G_R(t)$ simulations in Fig. 3(a) and (b), respectively. Also shown is the BPP prediction $G_R(t)$ from Eq. 11, generated with an arbitrarily chosen value of $\tau_R = 2$ ps. The y -axis has been divided by $G_R(0)$, which normalizes the area of the distributions to unity (except for the BPP model).

As a consistency check of the inverse Laplace algorithm and the resulting $P_{R,T}(\tau)$ distributions, it was verified that the predicted $\tau_{R,T}$ defined as:

$$\tau_{R,T} = \frac{1}{G_{R,T}(0)} \int P_{R,T}(\tau) \tau d\tau, \quad (14)$$

gave similar values as $\tau_{R,T}$ from Eq. 2. Indeed, the $\tau_{R,T}$ predicted from Eq. 14 was within $\pm 5\%$ of Eq. 2, for all the flexible molecules. In the case of the rigid n -alkanes however, Eq. 14 predicted (on average) a factor $\simeq 1.5$ longer $\tau_{R,T}$ compared to Eq. 2. For the rigid n -alkanes, this discrepancy is a result of the incomplete decay in

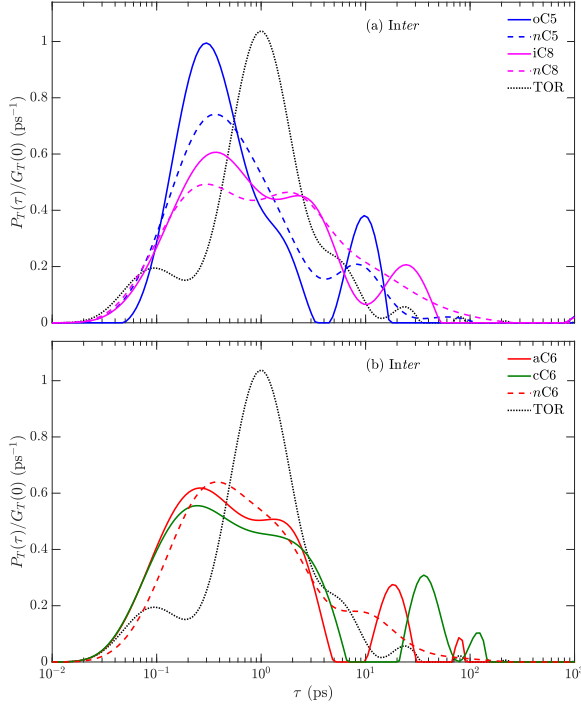


FIG. 18. Probability distribution function $P_T(\tau)$ of translational correlation time τ derived from the inverse Laplace transform (Eq. 8) of the $G_T(t)$ simulations in Fig. 4(a) and (b), respectively. Also shown is the Torrey (TOR) prediction $G_T(t)$ from Eq. 11, generated with an arbitrarily chosen value of $\tau_T = 2$ ps. The y -axis has been divided by $G_T(0)$, which normalizes the area of the distributions to unity.

$G_{R,T}(t)$ at $t = 150$ ps (Figs. 7 and 8), which tends to underestimate $\tau_{R,T}$ according to Eq. 2.

For completeness, Fig. 19 shows the $P_{R,T}(\tau)$ distributions for the complete set of flexible n -alkanes and water, where the $G_{R,T}(t)$ were previously reported in Ref. [1]. The case of water shows two distinct peaks in rotational distribution $P_R(\tau)$, which agrees well with previous reports [24, 25]. According to Ref. [25] for water, the larger peak ($\simeq 79$ % relative intensity) with longer rotational correlation-time ($\tau = 3.8$ ps) is interpreted as Debye continuous-time rotational diffusion, while the smaller peak ($\simeq 21$ % relative intensity) with shorter rotational correlation-time ($\tau = 0.22$ ps) is interpreted as large-amplitude discrete jumps.

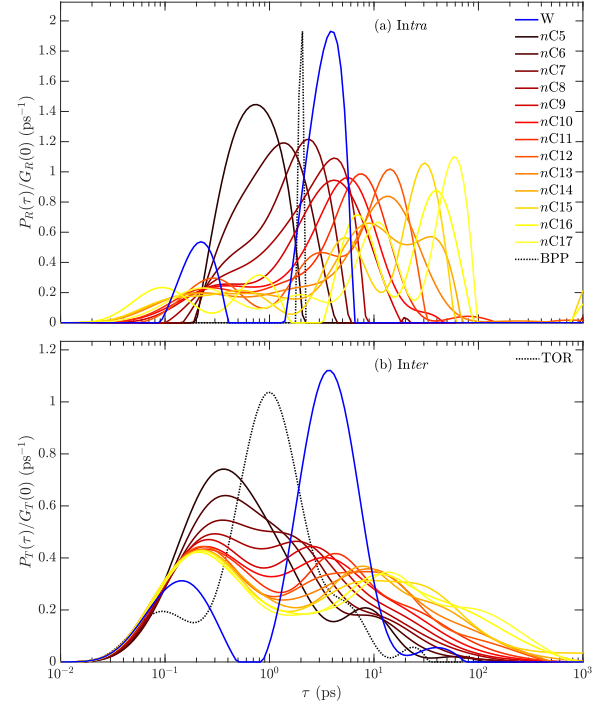


FIG. 19. Probability distribution function for (a) rotational $P_R(\tau)$ and (b) translational $P_T(\tau)$ correlation time τ derived from the inverse Laplace transform (Eq. 8) of the $G_{R,T}(t)$ simulations taken from Ref. [1], including water (W). Also shown are the BBP and Torrey (TOR) predictions $G_{R,T}(t)$ from Eq. 11, generated with an arbitrarily chosen value of $\tau_{R,T} = 2$ ps. The y -axis has been divided by $G_{R,T}(0)$, which normalizes the area of the distributions to unity (except for the BPP model).

SUPPLEMENTARY MATERIAL

Here we provide some background about cross-relaxation effects in liquids, and the definition of the T_1 and T_2 cross-relaxation rates $\sigma_{1,2,ij}$ between spin-pairs i and j , respectively. Cross-relaxation plays an important role in ^1H relaxation in liquids, and exact theories of cross-relaxation exist for the simple case of two-spin systems [3, 27, 63]. The case of n -heptadecane ($n\text{-C}_{17}\text{H}_{36}$) reported here consists of 36 ^1H spins for intramolecular

relaxation, and therefore presents a much more complex scenario than the two-spin case. However, we use the two-spin case to briefly explain the principles of cross-relaxation, and we neglect any possible cross-correlation effects with other relaxation mechanisms.

1. Longitudinal cross-relaxation

The time evolution of longitudinal magnetization for a two-spin system is solved using the well known Solomon equations [63]:

$$\frac{d}{dt} \begin{bmatrix} \langle \hat{I}_z \rangle \\ \langle \hat{S}_z \rangle \end{bmatrix} = - \begin{bmatrix} 1/T_{1,I} - \sigma_{1,IS} & \sigma_{1,IS} \\ \sigma_{1,IS} & 1/T_{1,S} - \sigma_{1,IS} \end{bmatrix} \begin{bmatrix} \langle \hat{I}_z \rangle - I_z^{eq} \\ \langle \hat{S}_z \rangle - S_z^{eq} \end{bmatrix}. \quad (15)$$

$$\frac{d}{dt} \begin{bmatrix} \langle \hat{I}_\pm \rangle \\ \langle \hat{S}_\pm \rangle \end{bmatrix} = - \begin{bmatrix} 1/T_{2,I} - \sigma_{2,IS} \mp i\delta_{IS}/2 & \sigma_{2,IS} \\ \sigma_{2,IS} & 1/T_{2,S} - \sigma_{2,IS} \pm i\delta_{IS}/2 \end{bmatrix} \begin{bmatrix} \langle \hat{I}_\pm \rangle \\ \langle \hat{S}_\pm \rangle \end{bmatrix}. \quad (16)$$

$\langle \hat{I}_z \rangle$ and $\langle \hat{S}_z \rangle$ are the time-dependent expectation values of the operators for longitudinal (i.e. z) magnetization for ^1H spins I and S along the chain, respectively. I_z^{eq} and S_z^{eq} are the equilibrium values of the longitudinal magnetization for ^1H spins I and S along the chain, respectively. $1/T_{1,I}$ and $1/T_{1,S}$ are the longitudinal relaxation rates for ^1H spins I and S , respectively. $\sigma_{1,IS}$ is the longitudinal cross-relaxation rate between ^1H spins I and S . According to Ref. [27], in the case of $\sigma_{1,IS} \ll \frac{1}{2}|1/T_{1,I} - 1/T_{1,S}|$, spins I and S relax at their own distinct rates [27], as would be predicted by the site-by-site simulations (e.g. #1, #2, etc.) in Fig. 16. In the opposite case of $\sigma_{1,IS} \gg \frac{1}{2}|1/T_{1,I} - 1/T_{1,S}|$, the two spins relax at the same rate given by the average $1/T_1 = \frac{1}{2}(1/T_{1,I} + 1/T_{1,S})$ defined in Eq. 13, as would be predicted by the ‘‘Ave’’ in Fig. 16.

When ^1H spins I and S are not identical (i.e. when their Larmor frequencies are not exactly equal $\omega_I \neq \omega_S$), one can manipulate the two spins independently and measure $T_{1,I}$, $T_{1,S}$ and $\sigma_{1,IS}$ using NOESY (nuclear Overhauser effect spectroscopy), and/or $T_{2,I}$, $T_{2,S}$ and $\sigma_{2,IS}$ (see below) using ROESY (rotating frame Overhauser effect spectroscopy), both at high magnetic-fields (typically $\omega_0/2\pi \gtrsim 100$ MHz) [3].

2. Transverse cross-relaxation

A slightly more complicated expression exists for the time evolution of transverse magnetization for a two-spin system [63] is given in Eq. 16, where $\langle \hat{I}_\pm \rangle$ and $\langle \hat{S}_\pm \rangle$ are the time-dependent expectation values of the operators

for transverse (i.e. x, y) magnetization for ^1H spins I and S along the chain, respectively, where step-up \hat{I}_+ and step-down \hat{I}_- operators are used ($\hat{I}_\pm = \hat{I}_x \pm i\hat{I}_y$). $1/T_{2,I}$ and $1/T_{2,S}$ are the transverse relaxation rates for ^1H spins I and S , respectively. $\sigma_{2,IS}$ is the transverse cross-relaxation rate between ^1H spins I and S . The additional term for transverse relaxation involves the frequency splitting $\delta_{IS} = |\omega_I - \omega_S|$ between the two ^1H sites, which for example a methyl (spin I) versus a methylene (spin S) is $\delta_{IS} \simeq 0.4$ ppm $\cdot \omega_0$ [65], or, $\delta_{IS}/2\pi \simeq 1$ Hz at $\omega_0/2\pi = 2.3$ MHz. Eq. 16 for T_2 is equivalent to Eq. 15 for T_1 , provided $\delta_{IS}/2 \lesssim \sigma_{2,IS}$ [3], which is the case here given that the measured T_1 and T_2 distributions are found to be roughly the same.

3. Fast-motion regime

Further insight can be obtained about the cross-relaxation rate $\sigma_{1,2,IS}$, given that the present case is in the fast-motion regime, i.e. $\omega_0 \tau_{R,T} \ll 1$. In the fast-motion regime, the following equalities hold: $T_{1,I} = T_{2,I}$, $T_{1,S} = T_{2,S}$, $\sigma_{1,IS} = \sigma_{2,IS}$, plus none of these quantities are dispersive (i.e. none depend on ω_0). One additional equality holds in the fast-motion regime, namely $\sigma_{1,2,IS} = \frac{1}{3}1/T_{1,2}$ [27], with the average defined as $1/T_{1,2} = \frac{1}{2}(1/T_{1,2,I} + 1/T_{1,2,S})$ from Eq. 13.

One can then loosely apply the above two-spin case in the fast-motion regime to the more complex case of n -heptadecane in Fig. 16(a); though this is a gross oversimplification, it can check whether our interpretation is at all reasonable. According to Fig. 16(a), the aver-

age $1/T_{1,2} \simeq 1.5 \text{ s}^{-1}$, which loosely implies that $\sigma_{1,2,IS} \simeq \frac{1}{3} 1/T_{1,2} \simeq 0.5 \text{ s}^{-1}$. The simulations further indicate that the spread is given by $\Delta_{1,2} \simeq |1/T_{1,I} - 1/T_{1,S}| \simeq 1.4 \text{ s}^{-1}$. Putting these two estimates together loosely indicates that $\sigma_{1,2,IS} \simeq \frac{1}{2} |1/T_{1,I} - 1/T_{1,S}| \simeq 0.5\text{-}0.7 \text{ s}^{-1}$, implying an intermediate cross-relaxation regime, which is quali-

tatively consistent with the findings in Fig. 16(a). Such consistency is motivation for a more thorough analysis of $\sigma_{1,2,ij}$ for all spin-pairs, provided extensions of Eqs. 15 and 16 are developed which (for instance) break down the 36 ^1H spin system into magnetization modes [3]. This is the first instance we are aware of where cross-relaxation effects can be studied by comparing simulations with measurements at low magnetic-fields ($\omega_0/2\pi \lesssim 2.3 \text{ MHz}$).

Name	Label	Rigid	$\Delta\omega_R/2\pi$ (kHz)	$\Delta\omega_T/2\pi$ (kHz)	τ_R (ps)	τ_T (ps)	τ_D/τ_R	σ_R	σ_T	$T_{1,2,T}/T_{1,2,R}$	$T_{1,2}$ (s)
neopentane	oC5		21.62	9.11	0.55	1.93	8.76	0.39	1.35	1.61	18.17
benzene	aC6		7.93	8.83	1.11	3.21	7.22	0.61	1.57	0.28	23.71
cyclohexane	cC6		17.86	10.55	1.43	7.40	12.90	0.86	1.87	0.56	5.93
isooctane	iC8		21.44	9.36	1.75	3.87	5.52	0.80	1.62	2.38	6.64
<i>n</i> -pentane	nC5		20.17	9.66	0.72	2.27	7.92	0.53	1.44	1.38	15.10
<i>n</i> -hexane	nC6		20.05	9.72	1.10	2.84	6.45	0.68	1.52	1.65	10.69
<i>n</i> -heptane	nC7		19.99	9.73	1.66	3.50	5.28	0.82	1.62	2.00	7.65
<i>n</i> -octane	nC8		19.93	9.73	2.45	4.30	4.38	1.02	1.72	2.40	5.50
<i>n</i> -nonane	nC9		19.87	9.76	3.34	5.19	3.88	1.21	1.84	2.67	4.19
<i>n</i> -decane	nC10		19.83	9.74	4.61	6.25	3.39	1.38	1.95	3.06	3.16
<i>n</i> -undecane	nC11		19.82	9.74	6.00	7.40	3.08	1.51	2.05	3.36	2.49
<i>n</i> -dodecane	nC12		19.80	9.73	8.22	10.57	3.22	1.59	2.15	3.22	1.80
<i>n</i> -tridecane	nC13		19.76	9.70	10.74	12.37	2.88	1.82	2.23	3.60	1.42
<i>n</i> -tetradecane	nC14		19.71	9.66	12.34	13.61	2.76	1.90	2.29	3.77	1.25
<i>n</i> -pentadecane	nC15		19.75	9.69	16.24	16.31	2.51	2.07	2.41	4.13	0.97
<i>n</i> -hexadecane	nC16		19.66	9.69	18.90	18.19	2.41	2.26	2.48	4.28	0.84
<i>n</i> -heptadecane	nC17		19.79	9.59	22.35	20.00	2.24	2.08	2.53	4.76	0.72
<i>n</i> -pentane	nC5	Rigid	19.77	9.83	1.31	2.13	4.07	1.01	1.38	2.48	10.58
<i>n</i> -hexane	nC6	Rigid	19.80	9.93	2.65	3.37	3.18	1.13	1.52	3.13	5.54
<i>n</i> -heptane	nC7	Rigid	19.53	10.05	6.77	5.81	2.14	1.40	1.68	4.40	2.40
<i>n</i> -octane	nC8	Rigid	19.59	10.13	16.42	8.19	1.25	1.85	1.82	7.50	1.06
<i>n</i> -nonane	nC9	Rigid	17.71	10.16	31.95	24.49	1.92	2.56	2.66	3.96	0.61
<i>n</i> -decane	nC10	Rigid	21.78	10.51	56.87	33.01	1.45	2.37	2.68	7.39	0.25

TABLE I. MD simulations results, including: fluid name, fluid label (chemical formula given in Fig. 1 caption), rigid or not, intramolecular dipolar strength $\Delta\omega_R/2\pi$ (Eq. 4), intramolecular dipolar strength $\Delta\omega_T/2\pi$ (Eq. 4), intramolecular correlation time τ_R (Eq. 2), intramolecular correlation time τ_T (Eq. 2), ratio of translational-diffusion to rotational correlation times τ_D/τ_R (where $\tau_D = \frac{5}{2}\tau_T$), intramolecular standard deviation σ_R (Eq. 9), intramolecular standard deviation σ_T (Eq. 9), ratio of intermolecular to intramolecular relaxation times $T_{1,2,T}/T_{1,2,R}$ (Eq. 6), and total relaxation time $T_{1,2}$ (Eq. 7).

Label	Site	Degen.	Rigid	$\Delta\omega_R/2\pi$ (kHz)	$\Delta\omega_T/2\pi$ (kHz)	τ_R (ps)	τ_T (ps)	τ_D/τ_R	σ_R	σ_T	$T_{1,2,T}/T_{1,2,R}$	$T_{1,2}$ (s)
<i>n</i> C17	#1	2		21.77	10.46	8.58	18.30	5.33	1.71	2.42	2.03	1.25
<i>n</i> C17	#2	4		21.71	10.50	8.47	18.13	5.35	1.68	2.41	2.00	1.27
<i>n</i> C17	#3	4		18.99	10.11	15.31	20.74	3.39	2.07	2.48	2.61	0.99
<i>n</i> C17	#4	4		18.99	9.91	21.13	22.44	2.66	2.17	2.50	3.46	0.77
<i>n</i> C17	#5	4		19.04	9.47	20.66	24.58	2.98	2.06	2.50	3.39	0.78
<i>n</i> C17	#6	4		19.22	9.24	26.53	25.67	2.42	2.10	2.52	4.48	0.63
<i>n</i> C17	#7	4		19.27	9.47	31.60	25.81	2.04	2.08	2.50	5.06	0.54
<i>n</i> C17	#8	4		19.48	9.52	32.75	26.08	1.99	2.10	2.52	5.26	0.51
<i>n</i> C17	#9	4		19.89	9.28	36.38	26.14	1.80	1.94	2.51	6.39	0.46
<i>n</i> C17	#10	2		19.55	9.58	34.18	24.78	1.81	1.89	2.46	5.75	0.50
<i>n</i> C10	#1	2		21.82	10.32	2.76	5.53	5.01	1.19	1.81	2.23	4.00
<i>n</i> C10	#2	4		21.75	10.31	2.97	5.54	4.66	1.16	1.81	2.39	3.81
<i>n</i> C10	#3	4		18.69	9.91	4.90	6.28	3.21	1.52	1.84	2.77	3.26
<i>n</i> C10	#4	4		18.85	9.65	4.48	6.74	3.77	1.43	1.86	2.53	3.43
<i>n</i> C10	#5	4		19.21	9.25	5.41	7.40	3.42	1.37	1.86	3.16	2.89
<i>n</i> C10	#6	4		19.30	9.19	5.62	7.55	3.36	1.39	1.87	3.29	2.78
<i>n</i> C10	#1	2	Rigid	20.97	10.18	44.23	27.23	1.54	2.28	2.60	6.90	0.34
<i>n</i> C10	#2	4	Rigid	21.69	10.28	47.67	27.74	1.45	2.33	2.62	7.65	0.30
<i>n</i> C10	#3	4	Rigid	20.01	10.56	60.37	30.97	1.28	2.31	2.66	7.00	0.28
<i>n</i> C10	#4	4	Rigid	21.85	10.53	61.67	35.35	1.43	2.43	2.70	7.51	0.23
<i>n</i> C10	#5	4	Rigid	22.76	10.66	59.60	36.13	1.52	2.39	2.70	7.53	0.22
<i>n</i> C10	#6	4	Rigid	22.84	10.71	60.70	37.05	1.53	2.34	2.70	7.45	0.21

TABLE II. Site-by-site MD simulations results, including: fluid label (chemical formula given in Fig. 1 caption), site number (Fig. 1), degeneracy, rigid or not, intramolecular dipolar strength $\Delta\omega_R/2\pi$ (Eq. 4), intramolecular dipolar strength $\Delta\omega_T/2\pi$ (Eq. 4), intramolecular correlation time τ_R (Eq. 2), intermolecular correlation time τ_T (Eq. 2), ratio of translational-diffusion to rotational correlation times τ_D/τ_R (where $\tau_D = \frac{5}{2}\tau_T$), intramolecular standard deviation σ_R (Eq. 9), intermolecular standard deviation σ_T (Eq. 9), ratio of intermolecular to intramolecular relaxation times $T_{1,2,T}/T_{1,2,R}$ (Eq. 6), and total relaxation time $T_{1,2}$ (Eq. 7).